



Universiteit  
Leiden  
The Netherlands

## **Holding the balance; the equilibrium between ER $\alpha$ -activation, epigenetic alterations and chromatin integrity**

Flach, K.D.

### **Citation**

Flach, K. D. (2018, September 25). *Holding the balance; the equilibrium between ER $\alpha$ -activation, epigenetic alterations and chromatin integrity*. Retrieved from <https://hdl.handle.net/1887/66110>

Version: Not Applicable (or Unknown)

License: [Licence agreement concerning inclusion of doctoral thesis in the Institutional Repository of the University of Leiden](#)

Downloaded from: <https://hdl.handle.net/1887/66110>

**Note:** To cite this publication please use the final published version (if applicable).

Cover Page



Universiteit Leiden



The handle <http://hdl.handle.net/1887/66110> holds various files of this Leiden University dissertation.

**Author:** Flach, K.D.

**Title:** Holding the balance; the equilibrium between ER $\alpha$ -activation, epigenetic alterations and chromatin integrity

**Issue Date:** 2018-09-25

# Chapter 5

## *Composition of ER $\alpha$ 's transcriptional complex – part 2*

### **Estrogen Receptor DNA-damage/methylation cycle as drug interface in tamoxifen resistant breast cancer by FEN1 blockade**

Koen Dorus Flach<sup>1</sup>, Manikandan Periyasamy<sup>2</sup>, Ajit Jadhav<sup>3</sup>, Theresa E. Hickey<sup>4</sup>, Mark Opdam<sup>5</sup>, Hetal Patel<sup>2</sup>, Sander Canisius<sup>6</sup>, David M. Wilson III<sup>7</sup>, Dorjbal Dorjsuren<sup>3</sup>, Marja Nieuwland<sup>8</sup>, Roel Kluin<sup>8</sup>, Alexey V. Zakharov<sup>3</sup>, Jelle Wesseling<sup>5</sup>, Lodewyk Frederik Ary Wessels<sup>6</sup>, Sabine Charlotte Linn<sup>5</sup>, Wayne D. Tilley<sup>4</sup>, Anton Simeonov<sup>3</sup>, Simak Ali<sup>2</sup>, Wilbert Zwart<sup>1</sup>

<sup>1</sup>Department of Oncogenomics, <sup>5</sup>Department of Molecular Pathology,

<sup>6</sup>Department of Molecular Carcinogenesis, <sup>8</sup>Genomics core facility, The Netherlands Cancer Institute, 1066 CX Amsterdam, The Netherlands.

<sup>2</sup>Department of Surgery and Cancer, Imperial College London, Hammersmith Hospital Campus, Du Cane Road, London W12 0NN, UK.

<sup>3</sup>National Center for Advancing Translational Sciences, National Institutes of Health, 9800 Medical Center Drive, MSC 3370, MD 20892, US.

<sup>4</sup>Dame Roma Mitchell Cancer Research Laboratories, Adelaide Medical School, Faculty of Health Sciences, DX Number 650 801, University of Adelaide, Adelaide, South Australia 5005, Australia.

<sup>7</sup>Laboratory of Molecular Gerontology, Intramural Research Program, National Institute on Aging, National Institutes of Health, Bayview Blvd 251, Baltimore, MD 21224, US.

*In submission*

**Abstract**

Estrogen receptor  $\alpha$  (ER $\alpha$ ) is a key transcriptional regulator in the majority of breast cancers. ER $\alpha$ -positive patients are frequently treated with tamoxifen, but resistance is common. Herein, a 111-gene outcome prediction-classifier was refined, revealing FEN1 as strongest determining factor in ER $\alpha$ -positive prognostication. We demonstrate FEN1 levels are predictive of outcome in tamoxifen-treated patients, and show FEN1 is required and sufficient for tamoxifen-resistance in ER $\alpha$ -positive cell lines. We show FEN1 dictates the transcriptional-activity of ER $\alpha$  by facilitating the formation and repair of hormone-induced DNA damage, ultimately resulting in DNA methylation changes. FEN1 blockade induced proteasome-mediated degradation of activated ER $\alpha$ , resulting in loss of ER $\alpha$ -driven gene expression and eradicated tumor cell proliferation. Finally, a high-throughput 460.000 compound screen identified a novel FEN1 inhibitor, which effectively blocks ER $\alpha$ -function and inhibits proliferation of tamoxifen-resistant cell lines as well as ex-vivo cultured ER $\alpha$ -positive breast tumors, providing therapeutic proof-of-principle for FEN1 blockade in tamoxifen-resistant breast cancer.

**Introduction**

Approximately 70% of all breast tumors are of the luminal subtype and their proliferation often depends on the activity of estrogen receptor  $\alpha$  (ER $\alpha$ ). Following estradiol (E2)-binding, a transcriptional complex is formed, initiated by Steroid Receptor Co-activator (SRC) p160 recruitment, which drives ER $\alpha$ -mediated transcription and cell proliferation programs (1).

Tamoxifen is often used in ER $\alpha$ -positive breast cancer patients, where it competitively blocks E2-binding, preventing co-activator-binding pocket formation and inhibiting cell proliferation (2). P160 member SRC3 (NCOA3, AIB1) is frequently amplified in breast tumors and correlates with a poor outcome after tamoxifen treatment (3).

Previously, we assessed the genome-wide chromatin binding landscape of all three p160 coactivators in MCF-7 breast cancer cells (4). Unique chromatin binding sites for each of the p160 family members were found, where genomic regions preferentially bound by SRC3 were uncovered proximal to 111 E2-responsive genes. Based on these genes, a prognostic classifier for outcome after tamoxifen treatment was developed. Which individual genes in the original classifier are critically involved in the observed clinical outcome remains elusive.

Besides recruitment of classic coregulators such as p160 proteins, DNA-modulating and DNA repair factors can also be recruited by ER $\alpha$  (5), as recently shown for APOBEC3B (6). APOBEC3B induces C-to-U deamination at ER $\alpha$  binding regions, leading to uracil DNA glycosylase (UNG) recruitment and ultimately to phosphorylation of H2AX at Serine 139 ( $\gamma$ H2AX) (6). While in theory the resulting UNG-mediated region of DNA that contains neither a purine nor a pyrimidine (abasic site), can be repaired by the Base Excision Repair (BER) pathway (7), however the exact interplay of BER proteins with ER $\alpha$  function remains unclear.

FEN1 is a member of the RAD2 nuclease family and cleaves overhanging flaps structures that arise during lagging-strand DNA synthesis (e.g. Okazaki fragments) (8) or long-patch BER, yielding a single-stranded DNA nick which can be ligated by DNA-ligase 1 (LIG1) (7). FEN1 deficiency predisposes to tumor development and FEN1 is upregulated in numerous tumor types, including breast cancer (9). Although endogenous ER $\alpha$ /FEN1 interactions have not been reported, incubation of immobilized FLAG-tagged ER $\alpha$  with MCF-7 nuclear extracts did identify FEN1 as an ER $\alpha$ -associating protein (10). Even though FEN1 was described as recruited to the TFF1 promoter and FEN1 knockdown resulted in reduced TFF1 mRNA expression, it remains

unknown whether FEN1 regulates estrogen responsiveness in a genome wide manner or by which mechanism. Additionally, FEN1 levels correlate negatively with overall survival in breast cancer (11), but whether ER $\alpha$ -status is the driving force behind this clinical observation remains unclear.

Here, we demonstrate that FEN1 dictates the transcriptional activity of ER $\alpha$  by facilitating the formation and BER of hormone-induced DNA damage, ultimately resulting in DNA methylation changes. The induction and processing of DNA damage by FEN1 is essential for ER $\alpha$ -activity, regulating responsive gene expression and ER $\alpha$ -induced cell proliferation. We demonstrate that FEN1 alters ER $\alpha$ 's activity by stabilizing chromatin interactions after activation. We show that FEN1 is a predictive marker of tamoxifen response in ER $\alpha$ -positive breast cancer patients, being both sufficient and essential for ER $\alpha$ -positive cell proliferation in the presence of tamoxifen. A novel small molecule inhibitor of FEN1 blocked tamoxifen resistant cell proliferation and primary ER $\alpha$ -positive tumor explants, yielding a novel therapeutic lead in the management of tamoxifen therapy resistance. Cumulatively, we present a pioneering proof-of-concept that spans from gene classifier and causal gene identification, to molecular mechanism, novel drug development and validation in ER $\alpha$ -positive breast cancer.

## **Results**

### **FEN1 levels correlate with breast cancer patient survival after tamoxifen treatment**

In a previous report, we identified 111 genes that predict outcome in tamoxifen-treated ER $\alpha$ -positive breast cancer patients (4). To reveal drivers causally involved in the observed patient outcome, we refined the gene signature to identify a minimal set of genes without losing predictive capacity (**Figure 1A**). Computationally minimizing the 111-gene classifier by Prediction Analysis for Microarrays (PAM) (12) and Lasso-penalized logistic regression (13) in two independent cohorts of tamoxifen-treated patients (14, 15) illustrated that the classifier could be reduced to four genes before losing its stratification potential: FEN1, MCM2, STARD13 and HBP1 (**Figure 1A**). Validation of the four genes in the METABRIC dataset (16) demonstrated that only FEN1 was significant by multivariate analysis in ER $\alpha$ -positive, but not ER $\alpha$ -negative cases (Sup Fig S1A), suggesting ER $\alpha$ -specific predictive potential of FEN1.

To assess the clinical impact of FEN1 as a single-gene classifier on

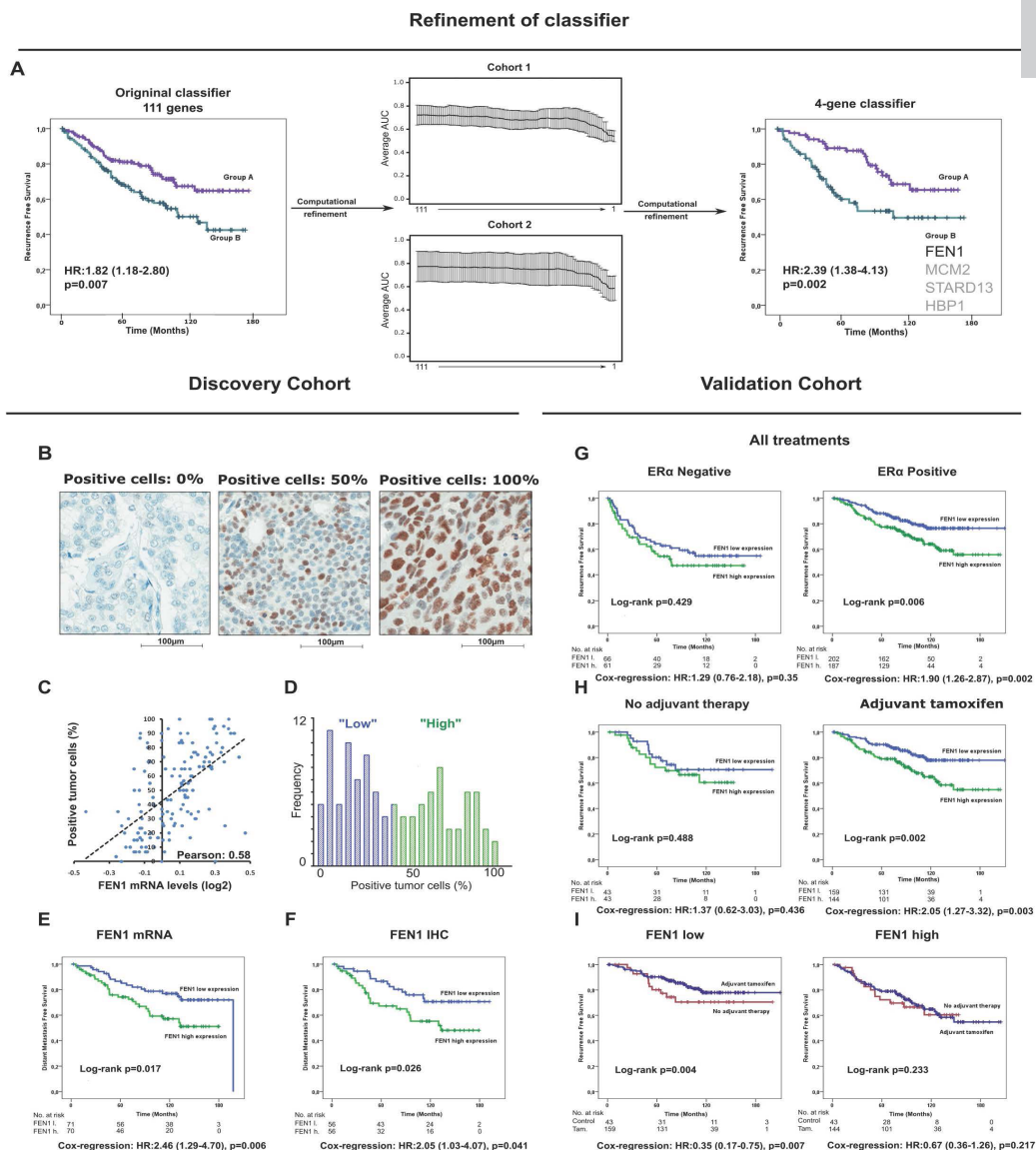


**Figure 1.** *FEN1* levels as predictive marker for tamoxifen response of breast cancer patients.

(A) Computational refinement of 111-gene classifier towards 4-gene classifier of *FEN1*, *MCM2*, *HBP1* and *STARD13*. PAM and Lasso-penalized logistic regression was performed to determine the minimum number of genes without affecting performance. (Left) Recurrence-Free Survival (RFS) of patients categorized according to

## Composition of ER $\alpha$ 's transcriptional complex – part 2

*III-gene classifier. Cox regression is shown. (Middle) Step-wise minimization of the III-genes with corresponding average area under the curve (AUC) in two cohorts. (Right) RFS of patients categorized according to 4-gene classifier. Cox regression is shown. See also Sup Fig S1A (B) Three representative IHC tumor cores, staining negative (0%), intermediate (50%) or entirely positive (100%) for FEN1. Scale bar is 100  $\mu$ m. (C) Scatterplot showing FEN1 mRNA levels (X-axis) related to FEN1 protein expression (% tumor cells, Y-axis), from the same tumor samples. Dotted line indicates trend line. Pearson correlation coefficient = 0.58. (D) Bar graph showing the individual IHC-scores for all tumor samples. Tumors were stratified in “Low” (IHC-score  $\leq$  36%) or “High” (IHC-score  $>$  36%) FEN1. (E) Distant Metastasis-Free Survival (DMFS) of tamoxifen-treated patients categorized according to FEN1 mRNA levels. Log-rank and Cox regression is shown. See also Sup table S1. (F) As in E, but now patients were categorized according to FEN1 IHC-score. (G) Randomized clinical trial: RFS of patients stratified by ER $\alpha$ -status and categorized according to FEN1 IHC-score. Log-rank and Cox regression is shown. See also Sup table S1 and Sup Fig S1B. (H) As in G, but now patients were stratified for adjuvant therapy (none or tamoxifen) and categorized according to FEN1 IHC-score. See also Sup table S1. (I) As in G, but now patients were stratified for FEN1 IHC-score and categorized according to adjuvant therapy (none or tamoxifen). See also Sup table S1.*

survival, we first used samples of ER $\alpha$ -positive cases that received adjuvant tamoxifen (Discovery-cohort) (17), using microarray-based (“mRNA”) and immunohistochemistry-based (“IHC”) FEN1 expression ranging from 0-100% positive tumor cells (**Figure 1B**), which correlated with FEN1 mRNA levels (Pearson correlation coefficient=0.58) (**Figure 1C**). For both mRNA and IHC, the median was used to stratify patients into “Low” and “High” FEN1 groups (**Figure 1D**). FEN1 mRNA (HR: 2.46, p=0.006) (**Figure 1E**) (Sup table S1) and protein (HR: 2.05, p=0.041) (**Figure 1F**) (Sup table S1) expression were associated with Distant Metastasis-Free Survival (DMFS), with high FEN1 levels correlating with a poor survival. These results were validated in an independent cohort, randomized between tamoxifen or no adjuvant endocrine therapy (Validation cohort) (18). This cohort contains a matched non-tamoxifen treated group, making it extremely useful to directly assess FEN1's tamoxifen specific predictive potential, providing an extra level of evidence not available from other tamoxifen cohorts that lack a non-treated control group (19).

In this cohort, FEN1 was associated with Recurrence-Free Survival

(RFS) in ER $\alpha$ -positive patients (n=389) (HR=1.90, p=0.002) (**Figure 1G**), also after multivariate correction for age, tumor grade, tumor stage, HER2, PgR and lymph node status (adjusted HR=1.58, p=0.047) (Sup Table S1), and confirmed in the METABRIC dataset (Sup Fig S1A,B). No association was found between FEN1 levels and RFS in ER $\alpha$ -negative breast cancer patients (n=127) (HR=1.29, p=0.35) (**Figure 1G** and Sup Fig S1B). Furthermore, high FEN1 significantly correlated with poor outcome in tamoxifen-treated patients (HR=2.05, p=0.003), but not for patients not receiving endocrine therapy (HR=1.37, p=0.436) (**Figure 1H**) (Sup table S1).

To further investigate whether FEN1 associates with disease progression (prognostic classifier) or whether its levels are informative for treatment response (predictive classifier), patients were stratified according to FEN1 levels and categorized by tamoxifen treatment (**Figure 1I**). Patients with high FEN1 did not benefit from tamoxifen (HR=0.67, p=0.217), while tamoxifen-treated patients with low FEN1 had a better survival (HR=0.35, p=0.007), also after multivariate correction (high FEN1 adjusted HR=0.67, p=0.213; low FEN1 adjusted HR=0.39, p=0.015) (Sup table S1).

As the standard regimens of hormonal treatment for ER $\alpha$ -positive breast cancer have changed since the time of our validation cohort, we tested how FEN1 levels would perform in a cohort using more contemporary hormonal therapies (METABRIC). In patients treated with hormonal therapy, high FEN1 was associated poor disease-specific survival (HR=2.09, p<0.001), also after multivariate correction (adjusted HR=1.83, p<0.001) (Sup Figure S1C). The predictive potential of FEN1 levels was further illustrated by the interaction test between FEN1 levels and hormonal therapy status (HR=2.19, p<0.001; adjusted HR=1.86, p<0.001) (Sup Figure S1C). Additionally, we assessed whether the menopausal status of a patient would influence the performance of FEN1 as predictive biomarker, as in the clinical setting tamoxifen is predominately used in pre-menopausal women. Both in premenopausal (HR=5.29, p<0.001) and postmenopausal patients (HR=1.79, p<0.001), FEN1 levels were significantly associated with patient outcome, also after multivariate correction (premenopausal adjusted HR=5.57, p<0.001; postmenopausal adjusted HR=1.62, p<0.001) (Sup Figure S1D).

In summary, FEN1 levels are not predictive of outcome in ER $\alpha$ -negative breast cancers, nor in ER $\alpha$ -positive disease in the absence of adjuvant endocrine therapy. Only in ER $\alpha$ -positive patients who were treated with tamoxifen FEN1 levels were negatively associated with outcome, rendering FEN1 a predictive marker for tamoxifen treatment response.

### FEN1 is essential for ER $\alpha$ -chromatin interactions and complex formation

FEN1 functions as a predictive marker for tamoxifen resistance in ER $\alpha$ -positive breast cancer. To determine whether FEN1 directly affects ER $\alpha$  activity, we tested if FEN1 is recruited to the ER $\alpha$  genomic complex. Based on co-immunoprecipitations, endogenous ER $\alpha$  and FEN1 interact in MCF7 cells, which is enhanced by E2 (**Figure 2A**). Knockdown of FEN1, as validated by western blot (Sup Fig 2A,B), abrogated ER $\alpha$ -chromatin interactions, which coincided with a loss of p300 binding (**Figure 2B,C,D** and Sup Fig S2C) and RNA Polymerase II (Sup Fig S2C) at these sites. FOXA1 chromatin binding (**Figure 2B,C,D**) and chromatin accessibility (**Figure 2E**) did not decrease by siFEN1, implicating FEN1 as a regulator of ER $\alpha$ -chromatin interactions downstream of FOXA1.

The main mode of action of FEN1 is 5' flap excision through its endonuclease activity (20), which is abrogated by the FEN1-D181A mutation (21). Overexpression of wild type FEN1 (FEN1-WT) enhanced ER $\alpha$ -chromatin interactions, while overexpression of FEN1-D181A (FEN1-dead) did not (**Figure 2F** and Sup Fig S2B), demonstrating that the nuclease activity of FEN1 is critical in regulating ER $\alpha$ -chromatin interactions.

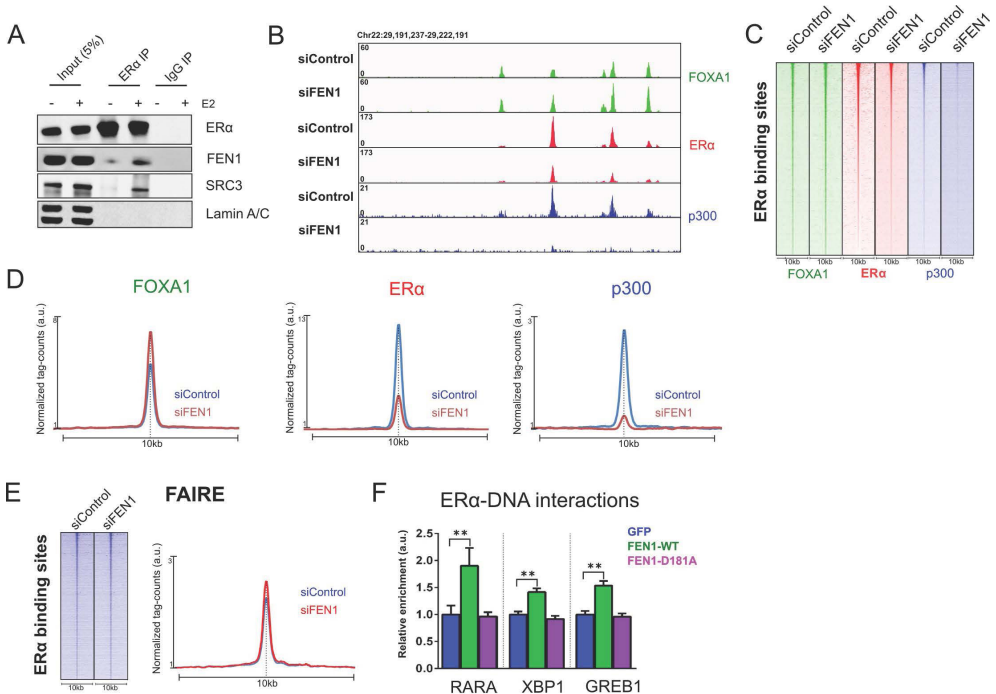


**Figure 2.** *FEN1 interacts with ER $\alpha$  and dictates ER $\alpha$ -chromatin interactions and complex formation.*

(A) Co-immunoprecipitation analyses demonstrate E2-induced ER $\alpha$ /FEN1 interactions. Protein levels were determined for ER $\alpha$ , FEN1, SRC3 and negative control Lamin A/C. Cells were treated with (+) or without (-) E2 before immunoprecipitation of ER $\alpha$  or IgG. Shown is an example of two biological replicates. (B) Genome browser snapshot at the XBP1 locus, illustrating FOXA1 (green), ER $\alpha$  (red) and p300 (blue) binding events for siFEN1 and control. Genomic coordinates and tag count are indicated. See also Sup Fig S2B,C. (C) Heatmap visualizing binding events of FOXA1 (green), ER $\alpha$  (red) and p300 (blue) at ER $\alpha$  binding sites after FEN1 knock-down. All binding events are vertically aligned and centered on the ER $\alpha$  peak, with a 10 kb window. Peaks were sorted on ER $\alpha$  intensity. See also Sup Fig S2B,C. (D) Normalized tag counts of FOXA1, ER $\alpha$  and p300 are plotted, showing average signal intensity within a 10kb window. (E) (Left) As in C but now binding events of Formaldehyde-Assisted Isolation of Regulatory Elements sequencing (FAIRE-seq) are visualized. Shown is an example of two biological replicates. (Right) As in D but now normalized tag counts of FAIRE are plotted. (F) ChIP-qPCR of ER $\alpha$  after overexpression of FEN1-WT (green), FEN1-D181A (purple) or control GFP (blue). ER $\alpha$ -bindings sites at enhancers proximal to XBP1, RARA and GREB1 were assessed. Signals are normalized over control genomics regions, after which siControl (blue) is set as 1. Shown is an example of three biological replicates.  $N=4$  with mean  $\pm$  SD. Henceforth asterisks: \*= $p$ -value $<0.05$ , \*\*= $p$ -value $<0.01$  and \*\*\*= $p$ -value $<0.001$  Students T-test. See also Sup Fig S2B,C.

### **FEN1 controls ER $\alpha$ -mediated transcription and cell proliferation**

The above results demonstrate that FEN1 modulates ER $\alpha$ -chromatin interactions and complex formation. Next, we assessed whether FEN1 can regulate ER $\alpha$ -mediated transcription and cell proliferation. Knockdown of FEN1 reduced ER $\alpha$ -regulated gene activation of known target genes TFF1, XBP1 and RARA (**Figure 3A**), while FEN1 overexpression had the opposite effect (**Figure 3B**), in line with increased ER $\alpha$ -chromatin binding (**Figure 2**).

FEN1 knockdown in MCF-7 cells decreased ER $\alpha$ -mediated cell growth under DMSO, tamoxifen and E2 conditions (**Figure 3C**; siRNA deconvolution in Sup Fig S3A), while FEN1 overexpression increased cell proliferation under these conditions (**Figure 3D**). The observed decrease in cell proliferation after siFEN1 was validated in ER $\alpha$ -positive T47D cells (Sup Fig S3B). Neither manipulating FEN1 levels in fulvestrant (a selective estrogen receptor down-regulator) treated cells, nor FEN1 knockdown in ER $\alpha$ -nega-

tive MDA-MB-231 and CAL120 cells (**Figure 3E**), affected cell proliferation, implicating that the observed effects are mediated through ER $\alpha$  and not broadly related to the role of FEN1 in DNA replication (20). Cumulatively, we demonstrate that FEN1 regulates ER $\alpha$ -mediated transcription and cell proliferation, and that FEN1 is both required and sufficient to dictate ER $\alpha$ -driven cell proliferation in the presence of tamoxifen.

### **FEN1 is required for the induction and BER of ER $\alpha$ -initiated DNA damage**

Given FEN1's key role in modulating ER $\alpha$ -activity, we hypothesized a FEN1 inhibitor used specifically in an ER $\alpha$ -positive setting could have great therapeutic potential. Since FEN1 inhibitors have been developed before on a small scale (22, 23) but were not effective in breast cancer cell lines on their own (24), we performed a small-molecule compound screen of over 460,000 compounds to identify novel inhibitors of FEN1's flap-cleaving activity. A previously reported non-radioactive FEN1 activity assay was used (25) in which a small DNA product containing fluorophore donor 6-TAMRA (6-Carboxytetramethylrhodamine) is cleaved and released by FEN1 from a DNA flap structure labeled with a fluorescent quencher (Black Hole Quencher 2), resulting in measurable fluorescence (**Figure 4A**). A quantitative high throughput robotics screen (26) was performed on 465,195 compounds (27), identifying 2,485 active FEN1 inhibitors (**Figure 4B** and Sup Fig S4A). As part of the NIH Molecular Libraries Program (<https://commonfund.nih.gov/molecularlibraries>), these compounds have been profiled for their effect in >150 biochemical and cell-based assays including DNA-repair and related screens (e.g. APE1, POLB, POLK, POLH, POLI, PCNA, DNA binding). Furthermore, cheminformatics filters have been applied to annotate compounds for their reactivity (28). The selectivity profiling data and filters for reactive functional groups were used to triage the 2,485 active FEN1 inhibitors, and a set of 22 inhibitors was selected for further biological validation.

After testing the 22 hits on MCF-7 cell proliferation, we continued with the three most potent hits for further validation (Sup Fig S4B). In line with the ER $\alpha$ -specific effect of FEN1 knockdown (**Figure 3**), we selected FENi#2 (MLS002701801) as most potent and promising hit, as this was the only compound to efficiently inhibit ER $\alpha$ -positive cells at 100 nM, but not ER $\alpha$ -negative MDA-MB-231 and CAL120 cells (**Figure 4B** and Sup Fig S4C) (Sup Table S2).

Since ER $\alpha$ -cofactor APOBEC3B can induce C-to-U modifications and

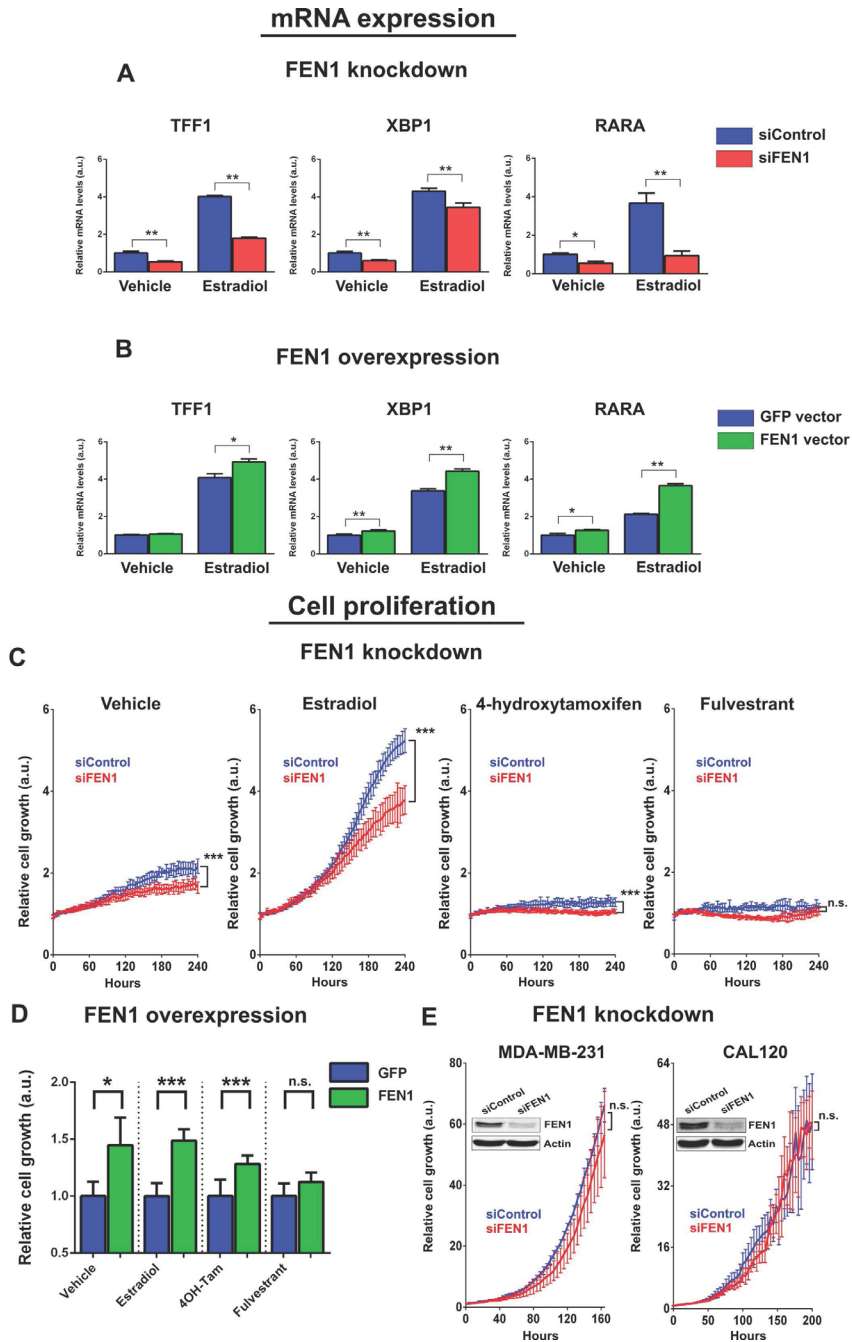


**Figure 3.** *FEN1* regulates ERα-mediated transcription and proliferation. (A) Relative mRNA levels of *TFF1*, *XBP1* or *RARA* with or without E2. TBP and

## *Composition of ER $\alpha$ 's transcriptional complex – part 2*

*UBC were used as controls. Cells were transfected with control siControl (blue) or siFEN1 (red). Shown is an example of three biological replicates. N=4 with mean  $\pm$  SD. (B) As in B, but now cells were transfected with exogenous FEN1 (green) or GFP control (blue). (C) Relative cell proliferation (Y-axis) over time (X-axis) of MCF-7 cells treated with vehicle, E2, tamoxifen or fulvestrant. Cells were transfected with control siRNA (blue) or siFEN1 (red). Relative growth was normalized over the number of cells at timepoint zero. Shown is a representative experiment of three biological replicates. N=6 with mean  $\pm$  SD with Students T-test at last time point. See also Sup Fig S3A. (D) Relative cell proliferation of MCF-7 cells treated with vehicle, E2, tamoxifen or fulvestrant. Cells were transfected with exogenous FEN1 (green) or GFP control (blue). Cell growth was normalized over GFP control after 150 hours of growth. Shown is a representative experiment of three biological replicates. N=6 with mean  $\pm$  SD. (E) As in C, but now MDA-MB-231 and CAL120 ER $\alpha$ -negative cells were grown in full medium. FEN1 and actin protein levels as assessed by western blot are depicted. Shown are representative experiments of two biological replicates. N=6 with mean  $\pm$  SD.*

UNG recruitment at ER $\alpha$  binding sites, which is essential for ER $\alpha$ -mediated transcriptional activity (6), we hypothesized that FEN1 might be functionally involved in a long-patch BER response following the formation of abasic sites, thereby regulating ER $\alpha$ -activity. In agreement with a BER response near ER $\alpha$ -binding sites, we observed BER-members XRCC1 and PARP1 (7), to bind these genomic regions (**Figure 4C** and Sup Fig S4D), with PARP1 being previously described as co-regulator of ER $\alpha$  (29). The targeted C-to-U events can ultimately give rise to  $\gamma$ H2AX formation at ER $\alpha$  sites (6), as assessed by ChIP-seq (**Figure 4D**). This  $\gamma$ H2AX-induction was validated by immunofluorescence, where E2 stimulation induced  $\gamma$ H2AX foci (**Figure 4E,F**). FEN1 inhibition through 100 nM FENi#2 blocked this E2-induced  $\gamma$ H2AX-formation (**Figure 4E,F** and Sup Fig S4E).

As  $\gamma$ H2AX is indicative of DNA damage, and BER of C-to-U sites would induce single stranded DNA nicks, we assessed whether FEN1 inhibition would affect E2-induced DNA damage. For this, we used biotin-16-deoxyuridine triphosphate (dUTP) labeling of DNA-breaks with terminal deoxynucleotide transferase (TdT) (30) followed by biotin ChIP-qPCR to directly assess DNA nicks. Consistent with previous reports (6, 30), biotin incorporation was increased 15 minutes after E2 stimulation, returning to basal levels at 30 minutes (**Figure 4G**). This induction was not seen at a non-ER $\alpha$ -binding region or with E2 stimulation in the absence of biotin-labeled dUTP. FEN1

Composition of ERα's transcriptional complex – part 2

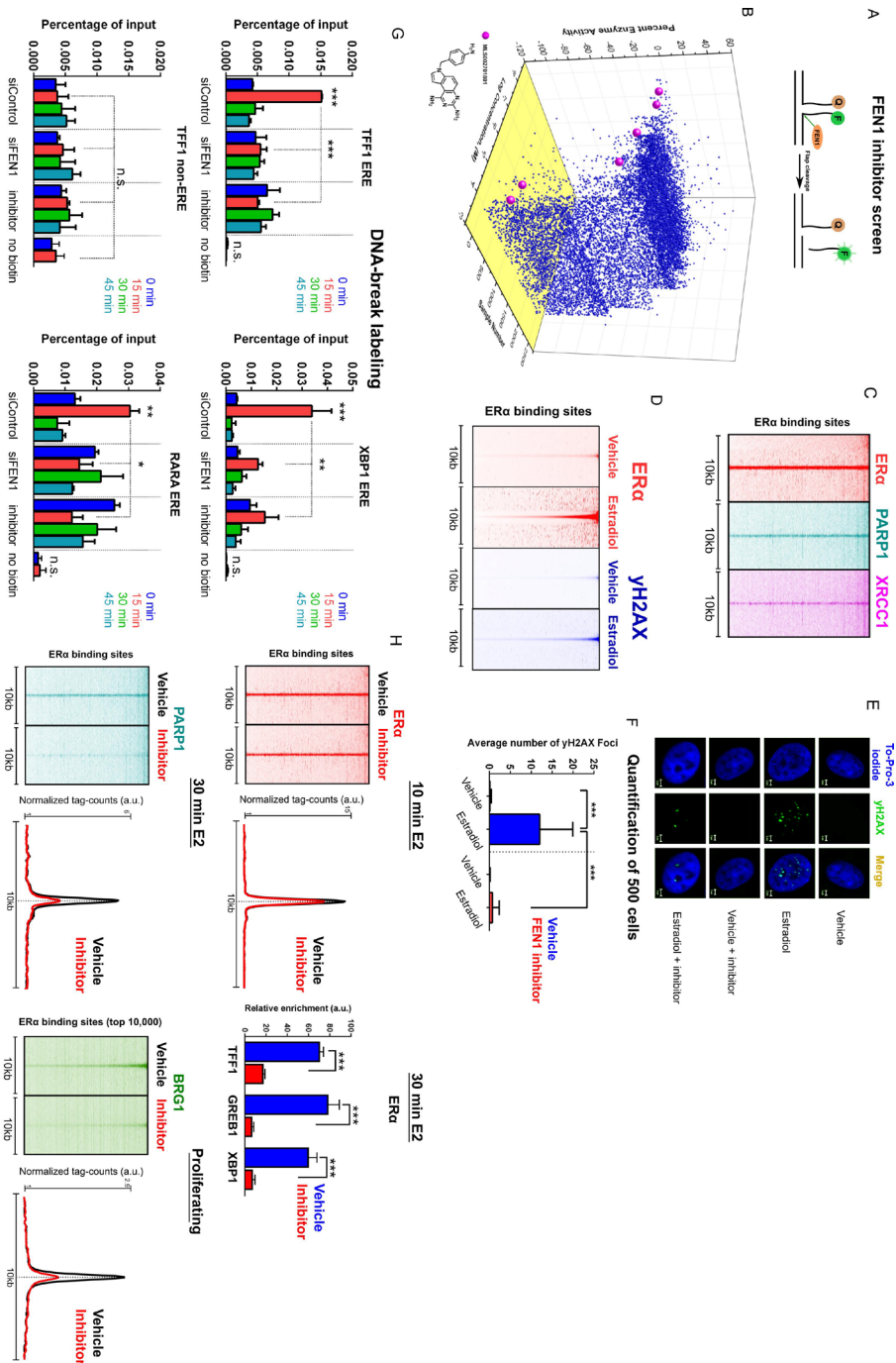


**Figure 4.** FEN1 inhibitor screen and the role of FEN1 in ERα-induced γH2AX signaling and DNA damage.

## Composition of ER $\alpha$ 's transcriptional complex – part 2

(A) Fluorescence based assay used to assess flap-cleaving by FEN1. A double-stranded DNA flap substrate containing two tags, a fluorophore-donor (6-TAMRA) and a fluorophore-quencher (BHQ2), is exposed to FEN1 protein in the presence or absence of small-molecule compounds. Upon flap-cleavage the DNA product containing the fluorophore is released, resulting in measurable fluorescence signal. (B) Concentration response profile of the 2,485 compounds found active as FEN1 inhibitors, identifying MLS002701801 (FENi#2) (purple dot) as our top hit. For each compound the concentration (log) and the percentage of altered FEN1 enzyme activity is depicted. See also Sup Table S2 and Sup Fig S4A,B,C. (C) Heatmap visualizing ranked binding events of ER $\alpha$  (red), PARP1 (dark cyan) and XRCC1 (purple) at ER $\alpha$  binding sites. Hormone-deprived cells were treated with E2 for 10 (ER $\alpha$  and XRCC1) or 30 minutes (PARP1). All binding events at ER $\alpha$  bound regions after 10 minutes of E2 were analyzed, vertically aligned and centered at the center of the peak, with a 10kb window. See also Sup Fig S4D. (D) As in C but now binding events of ER $\alpha$  (red) and  $\gamma$ H2AX (blue) at ER $\alpha$  binding sites, under vehicle or E2 conditions are visualized. Peaks were sorted on ER $\alpha$  intensity. (E) Induction of  $\gamma$ H2AX-foci by E2 stimulation as visualized through immunofluorescence. Hormone-deprived cells were treated with ethanol or E2 for 15 minutes, with or without FEN1 inhibitor. Shown is a representative cell stained for  $\gamma$ H2AX (green). To-Pro-3-iodide was used to visualize the nucleus (blue). Scale bar indicates 2 $\mu$ m. (F) The average number of  $\gamma$ H2AX-foci per cell as quantified in 500 cells. Shown is a representative experiment of two biological replicates. N=500 with mean  $\pm$  SD. See also Sup Fig S4E. (G) DNA-break labeling assay. Cells were transfected with siControl or siFEN1 or pretreated with a FEN1 inhibitor. Hormone-deprived cells were treated for 0, 15, 30 and 45 minutes of E2. Three ER $\alpha$ -binding sites and one non-ER $\alpha$ -binding site were investigated. No biotin was included as negative control. Shown is a representative experiment of two biological replicates. N=3 with mean  $\pm$  SD. (H) (Upper left) Heatmap visualizing ranked binding events of ER $\alpha$  (red) at ER $\alpha$  sites. Hormone-deprived cells were pretreated with a vehicle or FEN1 inhibitor and subsequently stimulated with E2 for 10 minutes. All binding events at ER $\alpha$  sites after 10 minutes of E2 were analyzed, vertically aligned and centered at the center of the peak, with a 10kb window. Normalized tag counts are plotted, showing average signal intensity. (Upper right) ChIP-qPCR analyses of ER $\alpha$  for enhancers proximal to TFF1, GREB1 and XBP1. Hormone-deprived cells were pretreated with a vehicle (blue) or FEN1 inhibitor (red) and stimulated with E2 for 30 minutes. Signal was normalized over control genomics regions. Shown is an example of three biological replicates. N=4 with mean  $\pm$  SD. (Bottom left) As in Upper left but now PARP1 binding sites were analyzed for cells stimulated with E2 for 30 minutes. (Bottom right) As in Upper left

but now BRG1 binding sites were analyzed for proliferating cells. See also Sup Fig S4F.

inhibition or siFEN1 blocked E2-mediated DNA damage induction (**Figure 4G**), suggesting FEN1 regulates ER $\alpha$ -activity through formation or processing of ER $\alpha$ -induced DNA damage. Reduced damage could not be explained by lower ER $\alpha$ -chromatin interactions at time points preceding DNA damage (10 minutes after E2 stimulation) (**Figure 4H** and Sup Fig S4F). However, after the point of damage induction (30 minutes of E2 stimulation), FEN1 inhibition did decrease ER $\alpha$  and PARP1 binding (**Figure 4H** and Sup Fig S4F), implicating the importance of BER-mediated DNA nicks in modulation of ER $\alpha$ -activity.

In line with the known role of  $\gamma$ H2AX in promoting chromatin remodeling (31), FEN1 inhibition decreased both  $\gamma$ H2AX formation and recruitment of BRG1; the catalytic subunit of the SWI/SNF chromatin remodeling complex (31) (**Figure 4H** and Sup Fig S4F), which chromatin interactions overlapped ER $\alpha$ -bindings sites.

FEN1 inhibition also enhanced E2-induced ER $\alpha$ -degradation (Sup Fig S4G), mediated by proteasomal activity (32). Pretreatment with proteasome inhibitor MG132 prevented FENi#2-induced reduction of ER $\alpha$ -chromatin interactions (Sup Fig S4G), suggesting that improper induction and processing of ER $\alpha$ -induced DNA damage through FEN1 blockade targets ER $\alpha$  for degradation. Since ER $\alpha$ -chromatin interactions are not affected by FEN1 inhibition until the point of damage induction (**Figure 4H** and Sup Fig S4F), this favors a model wherein FEN1 alters ER $\alpha$ 's activity by regulating the stability of its chromatin binding after activation by E2.

Cumulatively, we identified FENi#2 as a potent and specific FEN1 inhibitor, and demonstrate that FEN1 regulates ER $\alpha$ -activity through functional formation of E2-induced DNA damage. FEN1 inhibition reduced BRG1 recruitment and ultimately stimulated proteasome-mediated degradation of ER $\alpha$ .

### **FEN1 inhibition perturbs ER $\alpha$ mediated changes in DNA methylation**

Methylation status of ER $\alpha$  binding sites is tightly coupled with ER $\alpha$  activity (33), in which ER $\alpha$  activity was reported to induce TFF1 promoter demethylation (34), but whether this happens on a more genome-wide scale remains elusive. Since APOBEC3B-mediated C-to-U modifications at ER $\alpha$ -bound enhancers (6) appear to be repaired by the BER-pathway, and BER promotes DNA demethylation (35), we hypothesized that FEN1 is functionally involved

in genome-wide ER $\alpha$  DNA demethylation upon activation.

To investigate whether ER $\alpha$  activation triggers genome-wide DNA methylation changes through FEN1 action, we made use of Reduced Representation Bisulfite Sequencing (RRBS) (36) to map differentially methylated DNA regions after 45 minutes of E2 stimulation in the presence or absence of FEN1 inhibitor. RRBS allows for enrichment of genomic areas with a high CpG content, therefore including the majority of (potentially ER $\alpha$ -regulated) promoters.

Differential binding analyses identified 11,353 altered regions upon E2 stimulation, from which 418 high-confidence regions were selected by applying a stringent cutoff (minimum of ten methylation-informative bases and total methylation difference of at least  $\pm 20\%$ ). E2 stimulation triggered DNA methylation changes, ranging from  $\sim 82\%$  of hyper to  $\sim 73\%$  of hypomethylation, which was strongly reduced upon FEN1 inhibition (**Figure 5A,B quantified in C**). These regions were on average 203 bps, contained an average of 16 methylation-informative bases and were mainly located near gene promoters (**Figure 5D**). Of these 418 differentially methylated regions,  $\sim 53\%$  was  $< 20\text{kb}$  of an ER $\alpha$  site (**Figure 5D,E**). These ER $\alpha$ -associated regions contained 4570 methylation-informative bases, where altered methylation status upon E2 treatment ranged from  $\sim 48\%$  of hyper to  $\sim 47\%$  of hypomethylation (**Figure 5E**), which was fully abolished by FEN1 inhibition (**Figure 5F**). Cumulatively, we find that ER $\alpha$  activation induces changes in DNA methylation which are abrogated upon FEN1 inhibition.

### **FEN1 inhibition as novel drug option in tamoxifen resistant breast cancer**

Since tamoxifen-resistant cell lines (37) and tumors (38) still require ER $\alpha$  function, an alternative mode of blocking ER $\alpha$  action through FEN1 inhibition would have strong clinical potential.

First, the optimal time point of ER $\alpha$ -chromatin interactions after E2 treatment was determined, with 30 minutes of E2 stimulation resulting in maximum ER $\alpha$ -chromatin interactions (**Figure 6A** and Sup Fig S5A), consistent with previous TFF1 promoter-based studies (39). Overnight pretreatment with 100 nM FEN1 inhibitor significantly inhibited E2-induced ER $\alpha$ -chromatin interactions and ER $\alpha$ -driven gene transcription (**Figure 6B**) in MCF-7 cells, analogous to siFEN1 (**Figure 2, 3**). In the absence of E2, ER $\alpha$  protein levels were unaffected by the FEN1 inhibitor (Sup Fig S5B), indicating decreased ER $\alpha$ -chromatin interactions and gene transcription were not due to

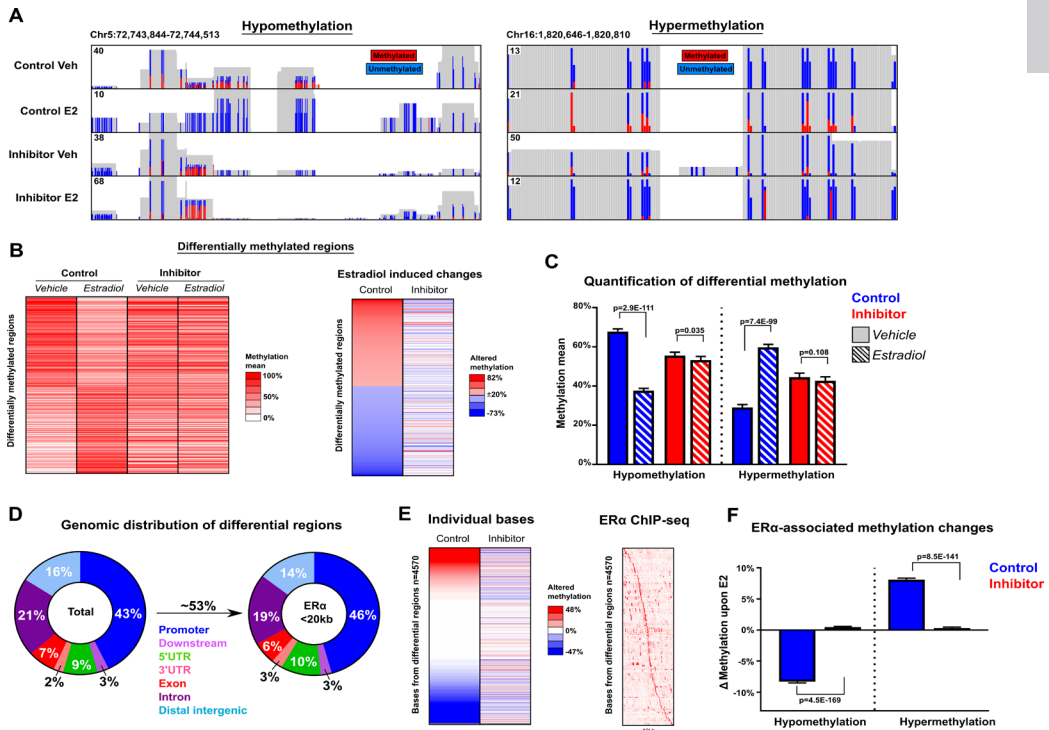


**Figure 5.** *FEN1* inhibition perturbs E2-stimulated differential DNA methylation. (A) Genome browser snapshot of RRBS at two loci, illustrating E2 induced hypo- (Left) and hypermethylation (Right). Colored bars indicate methylation-informative bases with corresponding methylated (red) and unmethylated (blue) reads. Genomic coordinates and tag count are indicated. Shown is one of two biological replicates. (B) (Left) Heatmap visualizing ranked differentially methylated regions upon E2 stimulation. The average methylation mean of two biological replicates is shown. (Right) As in Left but now percentage of altered methylation upon E2 stimulation is shown in the absence (control) or presence of *FEN1* inhibitor (inhibitor). (C) Quantification of the average methylation mean at the differential regions upon E2 stimulation in a control or inhibitor setting. Differential regions are split into hypo and hypermethylation. (D) Genomic distribution of all differentially methylated regions (Left) and regions <20kb of an ER $\alpha$  site (Right). (E) (Left) As in B but now altered methylation of individual methylation-informative bases from ER $\alpha$ -associated regions are shown. Shown is one of two biological replicates. (Right) Heatmap visualizing binding events of ER $\alpha$  at methylation-informative bases. All binding events are vertically aligned and centered on the individual bases, with a 20 kb window. Peaks were sorted on distance of ER $\alpha$  to individual bases. (F) Quantification of the average

## *Composition of ER $\alpha$ 's transcriptional complex – part 2*

*change in methylation of individual methylation-informative bases from E. Changes are split into hypo and hypermethylation.*

reduced initial amounts of ER $\alpha$  protein.

Colony formation assays were performed for a panel of human breast cancer cell lines; (a) MCF-7 and T47D (ER $\alpha$ +), (b) MCF7-T and TAMR (tamoxifen resistant MCF-7 derivatives (40, 41)) and (c) BT-20 and CAL-120 (ER $\alpha$ -). Cells were treated with increasing concentrations of FEN1 inhibitor in the presence or absence of tamoxifen (**Figure 6C,D**), confirming tamoxifen responsiveness of the sensitive cell lines (**Figure 6C,D**). Proliferation of MCF-7 and T47D cells was inhibited in a dose-dependent manner with IC<sub>50</sub> values of 69 and 78 nM of the inhibitor, respectively (Sup table S3). In contrast, sensitivity to FEN1 inhibition for ER $\alpha$ -negative cell lines BT-20 and CAL120 was limited, with an IC<sub>50</sub> of 314 nM in BT20, while not reaching 50% inhibition in CAL120 cells. Interestingly, tamoxifen resistant MCF-7 derivatives showed enhanced sensitivity to FEN1 inhibition in relation to the parental cells (IC<sub>50</sub>= 29 nM for both tamoxifen resistant cell lines).

To validate the efficacy of FEN1 inhibition in ER $\alpha$ -positive breast cancer, we used *ex vivo* primary ER $\alpha$ -positive tumor cultures (i.e. explants) (42, 43) in the presence or absence of compound FENi#2. Tumors were cut into small pieces and randomized between vehicle, FEN1 inhibitor or tamoxifen treatments and cultured for 3-6 days on gelatin sponges, allowing sustained tissue architecture and viability (43). Explants were stained for cell proliferation marker Ki67 and scored by a pathologist. Upon FEN1 inhibition, all four tumor explants demonstrated reduced proliferation (Ki67) (**Figure 6E,F**). For 3 of 4 explants, sufficient material was available for a tamoxifen group, demonstrating comparable reductions in Ki67 (Sup Fig S5C).

Taken together, we show that pharmacological inhibition of FEN1 efficiently blocks ER $\alpha$ -driven tumor cell proliferation, with enhanced potency in tamoxifen-resistant cells. As FEN1 perturbation inhibits primary tumor tissue growth, we demonstrate therapeutic potential of our FEN1 inhibitor in the treatment of ER $\alpha$ -positive cancer.

## **Discussion**

Several multi-gene prognostic classifiers have been reported that stratify breast cancer patients based on outcome (44). Most of these classifiers lack biological insights regarding the drivers of tumor progression. Here, we refined a 111-gene classifier to a single gene predictor of disease outcome, re-

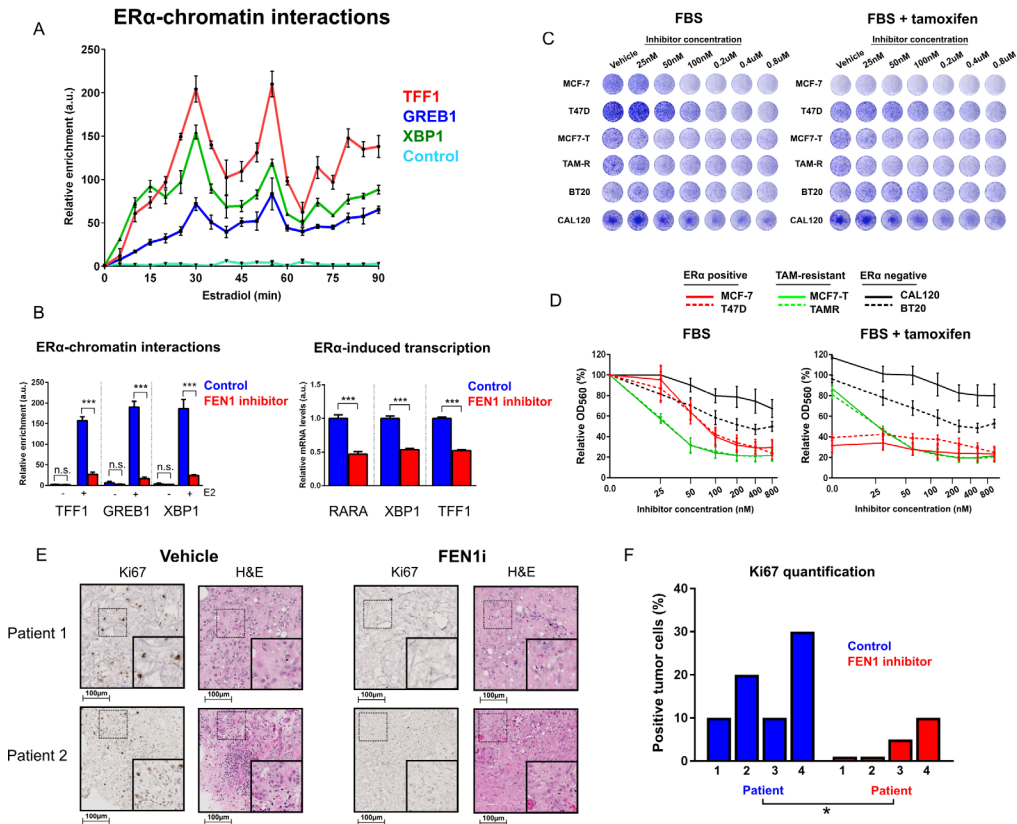


**Figure 6.** Small molecule-mediated inhibition of FEN1 blocks ER $\alpha$  action and prevents cell proliferation.

(A) ER $\alpha$  ChIP-qPCR analyses of hormone-deprived cells treated for 90 minutes with E2 using 5 minute intervals. Three positive regions for ER $\alpha$ -binding were assessed (TFF1, GREB1 and XBP1) and one known negative region (Neg control). Data are normalized over  $t=0$ .  $N=4$  with mean  $\pm$  SD. See also Sup Fig S5A. (B) (left) As in A but now hormone-deprived cells were pretreated with vehicle or FEN1 inhibitor prior to 30 minutes E2 treatment. Signals are normalized over control genomics regions. Shown is a representative experiment of two biological replicates.  $N=4$  with mean  $\pm$  SD. (right) Relative mRNA levels of RARA, XBP1 and TFF1 with or without FEN1 inhibitor. TBP and UBC were used as control. Shown is a representative experiment of two biological replicates.  $N=4$  with mean  $\pm$  SD. (C) Colony formation analyses for breast cancer cell lines; MCF-7 and T47D (ER $\alpha$ +), MCF7-T and TAMR (tamoxifen resistant MCF-7 derivatives) and BT-20 and CAL-120 (ER $\alpha$ -). Cells were treated with increasing concentrations of FEN1 inhibitor in the presence or absence

## *Composition of ER $\alpha$ 's transcriptional complex – part 2*

*of tamoxifen. Representative experiment is shown of at least 4 biological replicates. (D) Relative quantified crystal violet staining (OD560) of colony formation assay depicted in (C). Shown are mean values of at least 4 biological experiments where all OD560 data were normalized to vehicle treated FBS. Error bars indicate SEM. See also Sup table S3. (E) Ex vivo primary human ER $\alpha$ -positive tumor cultures in the presence or absence of 200 nM FEN1 inhibitor. Explants were fixed and stained for Ki67 and H&E. Shown are representative tumor regions for two patients with digital zoom in the lower right corner. (F) Indication of the percentage of Ki67 positive tumor cells in tumor explants cultured in the presence or absence of FEN1 inhibitor. Paired Students T-test was used to assess the difference between treatment groups. See also Sup Fig S5C.*

vealing a drug target with clinical potential in the treatment of tamoxifen resistant breast tumors. We identified FEN1 as a predictive marker for tamoxifen resistance in clinical specimens, with potential for outcome-prediction exclusive in ER $\alpha$ -positive breast cancers.

FEN1 overexpression is found in multiple tumor types, including breast cancer (9), in which it was reported to have prognostic potential (11). Our novel observation that FEN1 exclusively has prognostic potential in ER $\alpha$ -positive cases is in line with our cell proliferation analyses, where perturbation of FEN1 was only effective in ER $\alpha$ -positive cell lines, while yielding no detectable effects in ER $\alpha$ -negative cells. FEN1/ER $\alpha$  interactions were hormone-regulated and coincided with  $\gamma$ H2AX signaling at the same sites. At these genomic regions, the transcriptional activity of ER $\alpha$  appeared closely linked with the DNA damage response; a process in which FEN1's nuclease activity is required. The seemingly contradictory role of DNA damage repair protein FEN1 in the induction of DNA damage might be explained by it being part of a fail-safe mechanism, only allowing the induction of relevant damage intermediates when FEN1 is part of the ER $\alpha$  complex. A similar observation has been reported for DNA-dependent protein kinase (DNA-PK), where DNA-PK inhibition by NU7441 also resulted in the absence of  $\gamma$ H2AX formation upon ER $\alpha$ -activation (6). Consequently, this favors a model wherein FEN1 blockade reduces ER $\alpha$ -responsive gene expression and ER $\alpha$ -driven cell proliferation by deregulating ER $\alpha$ -chromatin interactions after activation by E2, most likely due to improper induction and processing of DNA damage.

Accumulating evidence repositions DNA repair factors as coactivators of transcription, facilitating chromatin remodeling (5). This chromatin remodeling at ER $\alpha$ -binding regions can be initiated by BRG1 (45), the recruit-

ment of which is promoted by  $\gamma$ H2AX (31). Failure to induce DNA damage at ER $\alpha$  regions diminished BRG1 recruitment (6), implicating ER $\alpha$ -induced damage as facilitator of chromatin remodeling. FEN1 is critically involved in ER $\alpha$ -mediated  $\gamma$ H2AX-formation, dictating BRG1 recruitment (**Figure 4H**) to regulate transcription. Additionally, chromatin-bound ER $\alpha$  can promote 8-oxoguanine modifications and thereby 8-oxoguanine-DNA glycosylase 1 recruitment and BER, triggering chromatin conformational changes essential for ER $\alpha$ -induced transcription (46). Together with APOBEC3B-mediated C-to-U modification at ER $\alpha$ -bound regions (6) and the fact that BER can promote DNA demethylation (35), we now show that BER upon ER $\alpha$ -stimulation induces active promoter demethylation; a process in which FEN1 is essential (**Figure 5**). Besides these regions of hypomethylation, we also find E2 stimulation yields regions of hypermethylation. As DNA methyltransferases have been reported to co-occupy ER $\alpha$ -interacting regions near the TFF1 and FOXA1 promoter (34, 47), the balance between methylating (e.g. DNMT's) and demethylating (e.g. FEN1's role in BER) proteins at ER $\alpha$ -binding sites may drive the directionality of DNA methylation alterations at these sites. Although not short-term E2 driven, differential hypermethylation between hormone-sensitive and endocrine resistant MCF-7 derivatives has been observed and proposed as possible mechanism for endocrine resistance and did result in differential ER $\alpha$ -binding capacities (48), further illustrating DNA methylation changes can regulate ER $\alpha$ -activity.

The role of FEN1 in ER $\alpha$ -induced transcription might be further explained by the fact that DNA nicks could resolve topological strain generated by transcription-induced DNA supercoiling, which, if unresolved, is able to affect transcription (49). Additionally, the known role of DNA damage repair proteins in the regulation of RNA-DNA hybrid structures (R-loops) (50) and their generation during ER $\alpha$ -induced transcription (51), is suggestive of a role for FEN1 in regulating ER $\alpha$ -induced transcriptional activity, DNA structures and genome instability.

Small molecule-mediated inhibition of FEN1 functionally abrogated ER $\alpha$ -activity and ultimately human tumor explant proliferation. With an inhibitor effective in the nM-range, we illustrate that FEN1 inhibition might yield a promising novel therapy for ER $\alpha$ -positive breast cancer. While FEN1 inhibition has been described before, it has mainly been linked to chemosensitization (52, 53) or as a part of synthetic lethal interactions (22, 54), but not as an effective therapy strategy on its own (24). Here we report the first effective single-agent application of FEN1 inhibition by specifically targeting

## *Composition of ER $\alpha$ 's transcriptional complex – part 2*

ER $\alpha$ -positive breast cancer. Most importantly, tamoxifen resistant cell lines showed an increased sensitivity for FEN1 blockade; a feature that could possibly be exploited in the treatment of advanced breast cancer, thereby providing a novel targeted therapy in case of tamoxifen resistance.

### **Materials and Methods**

#### **Colony formation**

For the colony formation assay 2500 cells/well were plated in 48-well format in appropriate culture medium. After attachment of cells to the bottom of the well, the FEN1 inhibitor was administered and when appropriate 100 nM 4OH-tamoxifen was added. After 7 days cells were fixed with 100% of methanol and cells were stained with 0.2% crystal violet. For quantification the crystal violet was dissolved in 10% acetic acid and the optical density was measured at 560 nm.

#### **Cell culture**

MCF-7, T47D, MDA-MB-231, CAL120 cells were cultured in DMEM medium in the presence of 10% FBS and antibiotics (penicillin, streptavidin). TAMR and MCF7-T cells were cultured in phenol-red-free DMEM containing 5% charcoal-treated serum (CTS; HyClone), 2 mmol/L of L-glutamine, antibiotics and 100 nM 4OH-tamoxifen. BT20 cells were cultured in MEM in the presence of 10% FBS and antibiotics. For hormone deficient conditions, cells were deprived of hormone for 72 hours, by culturing in phenol-red-free DMEM containing 5% charcoal-treated serum, antibiotics and supplemented with L-glutamine, prior to hormone treatment. Hormone treatments consisted of solvent Dimethylsulfoxide (DMSO), 10 nM of estradiol, 100 nM of 4OH-tamoxifen or 100 nM of fulvestrant. All cell lines were tested for mycoplasma and were genotyped for authenticity.

#### **siRNA and plasmid**

For knockdown experiments 25 nM of single or pooled duplexes of siRNA against FEN1 (Dharmacon MU-010344-01) or a non-targeting control pool (Dharmacon, D-001206-14-20) were transfected with Dharmafect according to manufactures protocol. The expression plasmids pShuttle-FEN1hWT (wild type FEN1) and pShuttle-FEN1DA (D181A point mutant) were kindly provided by Sheila Stewart (Addgene plasmid #35027 and #35028) (21) and cells were transfected with Polyethylenimine (PEI). When appropriate cells

were hormone-deprived for 24 hours prior to siRNA transfection or overexpression and further hormone-deprived for 48-72 hours.

### **Chromatin Immunoprecipitation (ChIP) and Formaldehyde-assisted isolation of regulatory elements (FAIRE)**

ChIP experiments were performed as described previously (4) with the following modifications. Three to ten micrograms of antibody was prebound overnight to protein A Dynabeads magnetic beads (Invitrogen). The magnetic bead-chromatin complexes were harvested and washed 10 times with RIPA buffer (50 mM HEPES [pH 7.6], 1 mM EDTA, 0.7% Na deoxycholate, 1% NP-40, 0.5 M LiCl). Antibodies used were anti-ER $\alpha$  (sc-543), anti-p300 (sc-585), anti-FOXA1 (sc-6554), anti-BRG1 (sc-10768), anti-PARP1 (sc-1561) from Santa Cruz Biotechnologies and anti-RNA polymerase II (ab5408), anti-XRCC1 (ab9147) from Abcam. In figure 4, publically available ChIP-seq data was used; ER $\alpha$  (37) and  $\gamma$ H2AX (GSE57426) (6). Formaldehyde-assisted isolation of regulatory elements (FAIRE) was performed as described previously (55).

### **Solexa ChIP and FAIRE sequencing and enrichment analysis**

ChIP DNA was amplified as described (56). Sequences were generated by the Illumina HiSeq 2000 genome analyser (using 51 or 65 bp reads), and aligned to the Human Reference Genome (assembly hg19, February 2009). Peak calling over input was performed using MACS peak caller (57) version 1.3.7.1 and DFilter (58), only considering peaks shared by both peak callers. For Figure 2B and Figure 4C all ER $\alpha$  binding regions after 45 minutes of estradiol as published before (37) were used. Details on the number of reads obtained and the percentage of reads aligned can be found below. ChIP-seq and FAIRE-seq data can be found on GEO: GSE95302

### **Sequencing snapshots and Heatmaps**

ChIP-seq and RRBS data snapshots were generated using the Integrative Genome Viewer IGV 2.2 ([www.broadinstitute.org/igv/](http://www.broadinstitute.org/igv/)). Heatmaps were generated using Seqminer, with default settings (59).

### **Characteristics of ER $\alpha$ and $\gamma$ H2AX ChIP-Seq data**

ChIP Published

ER $\alpha$  vehicle E-MTAB-223 (Hurtado et al., 2011)

ER $\alpha$  estradiol E-MTAB-223 (Hurtado et al., 2011)

## Composition of ER $\alpha$ 's transcriptional complex – part 2

$\gamma$ H2AX vehicle            GSE57426 (Periyasamy et al., 2015)  
 $\gamma$ H2AX estradiol        GSE57426 (Periyasamy et al., 2015)

### Characteristics of ChIP-Seq and FAIRE-seq samples

| ChIP                                 | Total count | tag # tags after filtering | % of tags after filtering |
|--------------------------------------|-------------|----------------------------|---------------------------|
| ER $\alpha$ siControl                | 7781308     | 7438883                    | 95.6                      |
| ER $\alpha$ siFEN1                   | 14756460    | 13972667                   | 94.7                      |
| P300 siControl                       | 7175975     | 6987295                    | 97.4                      |
| P300 siFEN1                          | 12257252    | 11672856                   | 95.2                      |
| FOXA1 siControl                      | 19374850    | 15196594                   | 78.4                      |
| FOXA1 siFEN1                         | 14684955    | 13312265                   | 90.7                      |
| FAIRE siControl                      | 20840022    | 18945798                   | 90.9                      |
| FAIRE siFEN1                         | 19089826    | 17367171                   | 90.9                      |
| ER $\alpha$ 10 min E2 vehicle        | 27769120    | 26639560                   | 95.9                      |
| ER $\alpha$ 10 min E2 FEN1 inhibitor | 26580604    | 25540190                   | 96.0                      |
| XRCC1 10 min E2                      | 25039992    | 23979349                   | 95.7                      |
| PARP1 30 min E2 vehicle              | 24826707    | 22424144                   | 90.3                      |
| PARP1 30 min E2 FEN1 inhibitor       | 25045100    | 23528730                   | 93.9                      |
| BRG1 control                         | 21291086    | 20282090                   | 95.3                      |
| BRG1 fen1 inhibitor                  | 21350779    | 19952407                   | 93.5                      |

### mRNA expression and ChIP-qPCR

For mRNA expression; after hormone deprivation cells were treated for 6 hours with DMSO or 10 nM estradiol, after which total RNA was collected by phenol-chloroform extraction. cDNA was made with a Superscript III RT kit (Invitrogen) using manufacturer's protocols after which qPCR was performed. TBP and UBC were used as housekeeping genes. For ChIP: DNA-protein interactions were harvested with ChIP and obtained DNA regions were used after immunoprecipitation. qPCR was performed with SYBR Green (Applied Biosystems) on a Roche LightCycler® 480 Real-Time PCR System using standard protocols. A negative region near the cyclin D1 (CCND1) promoter was used as a negative control. When appropriate an additional negative control primer (Neg 2) was taken along. Primers are described below.

**Primers cDNA**

| Gene                                 | Sequence   |
|--------------------------------------|--|
| Homo sapiens trefoil factor 1 (TFF1) | ATCGACGTCCCTCCAGAAGA (FWD)<br>TGGGACTAATCACCGTGCTG (REV) |
| X-box binding protein 1 (XBP1)       | GGGAAGGGCATTGAAGAAC (FWD)<br>ATGGATTCTGGCGGTATTGA (REV)  |
| retinoic acid receptor alpha (RARA)  | GACCAGATCACCTCCTCAA (FWD)<br>GTCCGAGAAGGTCATGGTGT (REV)  |
| TATA box binding protein (TBP)       | GTTCTGGGAAAATGGTGTGC (FWD)<br>GCTGGAAAACCCAATTCTG (REV)  |
| ubiquitin C (UBC)                    | ATTTGGGTCGCAGTTCTTG (FWD)<br>TGCCTTGACATCTCGATGGT (REV)  |

**Primers ChIP**

| Gene   | Sequence  |
|--|---|
| cyclin D1 (CCND1) (Neg 1)                                | TGCCACACACCAGTGACTTT (FWD),<br>ACAGCCAGAAGCTCCAAAAA (REV) |
| Homo sapiens trefoil factor 1 (TFF1)                     | TGGTCAAGCTACATGGAAGG (FWD)<br>CCATGGGAAAGAGGGACTTT (REV)  |
| growth regulation by estrogen in breast cancer 1 (GREB1) | CACTTTGAGCAAAAGCCACA (FWD)<br>GCTGCGGCAATCAGAAGTAT (REV)  |
| X-box binding protein 1 (XBP1)                           | GGTCACAGGCTGCCAAGTAT (FWD)<br>AGCCCCAGTTATGGCGTAAT (REV)  |
| retinoic acid receptor alpha (RARA)                      | CTCAGGACAGGGCAAGAGTG (FWD)<br>AAGCCACTCCAAGGTAGGTG (REV)  |
| Negative control 2 (Neg 2)                               | TGGCCCTTGATACTGGAGTC (FWD)<br>GACATCCAAGGCAAGATGGT (REV)  |
| PDZ Domain Containing 1 (PDZK1)                          | AGGCCAGCAAAGACAAATG (FWD)<br>AAACCACAGGCTGAGGACTG (REV)   |

**Co-Immunoprecipitation**

Immunoprecipitations were performed as described previously (60). MCF-7 cells were lysed in RIPA whole cell lysate buffer containing protease inhibitors. Lysates were pre-cleared by incubating with pre-clearing beads (Immunocruz, Santacruz) at 40C for 2 hours. 5 $\mu$ g of ER $\alpha$  antibody (ER HC20) was incubated with agarose beads (Immunocruz, Santacruz) for 2 hours at 40C. Agarose beads conjugated with ER $\alpha$  antibody were washed three times with ice-cold PBS and re-suspended in PBS and transferred to the pre-cleared lysates for overnight incubation. Following incubation, beads were washed six times in ice-cold PBS and re-suspended in 2X sample buffer (Sigma, 0.125 M Tris-HCL at pH 6.8, 4% SDS, 20% Glycerol, 10%  $\beta$ -mercaptoethanol and 0.004% bromophenol blue) and heated at 950C for 10 minutes, and then analyzed by western blot. Antibodies used for IP; anti-ER $\alpha$  (sc-543) from Santacruz, and for WB; anti-ER $\alpha$  (6F11) from Leica Biosystems, anti-AIB1 (BD

## *Composition of ER $\alpha$ 's transcriptional complex – part 2*

bioscience, cat no; 611105) and anti-Lamin A/C (sc-7292) and anti-FEN1 (sc-28355) from SantaCruz.

### **Western blot**

Cells were lysed with 2x laemmli buffer (containing 1:500 Na<sub>3</sub>VO<sub>4</sub>, 1:10 NaF, 1:13  $\beta$ -Glutamate, 1:100 Protease inhibitors, 1:100 Phosphatase inhibitors). Western blot samples contained 10% DTT and 4% bromophenol blue and were incubated for 5 minutes at 95 °C. Samples were run on 10% SDS-Page gel and transferred to nitrocellulose membranes. Used primary antibodies: anti-p300 (sc-585), anti-FOXA1 (sc-6554), anti-ER $\alpha$  (sc-543) and anti-FEN1 (sc-13051) from Santa Cruz Biotechnologies, anti-RNA polymerase II (ab5408) from Abcam and 1:10.000 actin from Millipore (MAB1501R). Used secondary antibodies: 1:10.000 Licor Odyssey IRDye. Membranes were scanned and analysed with Odyssey V3.0.

### **Patient cohorts**

The discovery-cohort has previously been used and described (17). In short; ER $\alpha$ -positive patients that received tamoxifen in the adjuvant setting, but did not receive adjuvant chemotherapy, were selected from The Netherlands Cancer Institute–Antoni van Leeuwenhoek Hospital (NKI–AVL). Distant metastases were regarded as failure to treatment and used as events. RNA was hybridized on 44 K oligomicroarrays, as described previously (61). The median IHC-score and mRNA expression value was chosen as the cutoff-point.

The validation-cohort has been described before (IKA trial, 1982-1994) (18). In short: ER $\alpha$ -positive patients (no adjuvant chemotherapy) were randomized between 1 year tamoxifen versus no adjuvant therapy. After 1 year a second randomization was performed; 2 additional years of tamoxifen or to stop further treatment. Further patient characteristics and clinical outcome of the original study group (1662 patients) have been described before (62). For 739 patients sufficient tumor material for IHC was available (62). The median IHC-score value was chosen as the cutoff-point.

### **Immunohistochemistry**

Tissue microarrays (TMAs) were constructed using formalin-fixed paraffin embedded (FFPE) tumor blocks. A total of three (0.6 mm) cores per tumor were embedded in the TMA. TMAs were stained for FEN1 and hematoxylin-eosin (HE) with the ULTRA BenchMark IHC/ISH Staining Module of the NKI. Antibody used was anti-FEN1 (sc-13051) from Santa Cruz Biotechnol-

ogies. The percentage of FEN1-positive invasive tumor cells were scored. One TMA was scored independently in a blinded manner by a second observer to calculate inter-observer variability ( $\kappa=0.708$ ). The inter-observer variability was analyzed using the (weighted) Cohen's kappa coefficient.

For ex-vivo tumor cultures, tissue sections were incubated with a Ki67 primary antibody (MIB1 1:400; DAKO M7240 Glostrup, Denmark) at 4C overnight followed by detection using a biotinylated anti-mouse secondary antibody at 1:400 dilution (DAKO E0433, Glostrup, Denmark) for 30 min followed by incubation with horseradish peroxidase-conjugated streptavidin (DAKO P0397, Glostrup, Denmark). Visualization of immunostaining was performed using 3,3-diaminobenzidine (Sigma D9015).

### Statistics

PAM (12) was performed to determine the minimum number of genes required to attain accurate separation of good and poor survival. Here, good and poor survival was defined based on whether or not a distant metastasis occurred within five years. The number of genes was selected such that the area under the ROC curve (AUC) was optimized in a 10-fold cross validation. Subsequently, Lasso-penalized logistic regression (13) was used to obtain a robust selection of the best performing genes across two cohorts (14, 15). To this end, 1,000 cross-validation analyses were performed for each cohort to select gene subsets optimizing the AUC. Genes were then ranked according to how many times they were part of the optimal gene set in either of the two cohorts. Finally, the previously determined optimal number of genes were selected starting from the highest ranked gene.

Pearson's correlation coefficient was used to assess the correlation between relative FEN1 mRNA levels and FEN1 IHC scores. Survival curves were constructed using the Kaplan-Meier method and compared using log-rank test. Unadjusted and adjusted Cox proportional hazard regression analyses were performed; for the discovery-cohort the covariates age (<60 versus  $\geq 60$ ), diameter of the tumor ( $\leq 20$  mm versus 20-50 mm versus >50 mm), tumor grade (grade 1 versus grade 2 versus grade 3) and the number of affected lymph nodes (Negative versus 1-3 versus  $\geq 4$ ); and for the validation-cohort the covariates age (< 65 versus  $\geq 65$ ), grade (grade 1-2 versus grade 3), tumor stage (T1-T2 versus T3-4), HER2 status (negative versus positive), PgR status (negative versus positive). In the validation-cohort all analyses were stratified for nodal status (negative versus positive) because lymph node positive patients, after 1989, skipped the first randomization and all received 1

## Composition of ER $\alpha$ 's transcriptional complex – part 2

year of tamoxifen. A p-value <0.05 was considered as a significant result and FEN1 levels were used a binary factor to assess the interaction with adjuvant treatment. A two-tailed Student's t-test was performed when appropriate.

### Biotin labeling of DNA strand breaks

Biotin labelling of DNA strand breaks was performed as described (6, 30). MCF-7 cells were hormone deprived for 3 days before the addition of 10 nM estradiol (0, 15, 30 or 45 minutes treatment). Additionally cells were transfected with siRNA against FEN1 or pretreated with 100 nM of FEN1 inhibitor as appropriate. Real-Time PCR System using standard protocols. Primers are described below.

| Gene                                 | Sequence   |
|--------------------------------------|--|
| Homo sapiens trefoil factor 1 (TFF1) | CCCGTGAGCCACTGTTGT (FWD)<br>ATGGGAGTCTCCTCCAACCT (REV)   |
| Non ERE control near TFF1            | TAAAGTGATCCGCCTGCTTT (FWD)<br>ATGGGAGTCTCCTCCAACCT (REV) |
| X-box binding protein 1 (XBP1)       | GGTCACAGGCTGCCAAGTAT (FWD)<br>AGCCCCAGTTATGGCGTAAT (REV) |
| retinoic acid receptor alpha (RARA)  | CTCAGGACAGGGCAAGAGTG (FWD)<br>AAGCCACTCCAAGGTAGGTG (REV) |

### Immunofluorescence

Immunofluorescence analysis was performed as described previously (6). Briefly, hormone-deprived MCF-7 cells were cultured on glass coverslips before the addition of 10 nM E2. Additionally cells were pretreated with 100 nM of FEN1 inhibitor as appropriate. Cells were fixed with 4% paraformaldehyde for 10 minutes and permeabilized with 0.2% Triton X-100. Used primary antibody was  $\gamma$ H2AX (05-636, Millipore) and for secondary Alexa fluor 488 (Invitrogen) was used. ToPro (Invitrogen) nuclear dye was used to visualize nuclei. Images were acquired using a Carl Zeiss confocal microscope using LSM 510 image browser. Images were analyzed using Fuji Image J (NIH, USA) and Cell Profiler (Broad Institute, USA) to quantify number of foci per cell.

### FEN1 inhibitor Screen

The previously reported non-radioactive FEN1 activity assay (25) was combined with a quantitative high throughput screen (qHTS) (26) and implemented on a fully integrated robotic system (63), utilizing a large scale chemical library arrayed in qHTS-formatted 1536-well based plates (27). A total of 465,195 compounds were tested. Automated large-scale curve fitting and

classification of curve types were determined (26). Using this classification, 3,543 compounds were considered inconclusive or weak inhibitors due to either lower quality curves or moderate inhibition. Another 1,123 compounds demonstrated a dose dependent increase of fluorescent signal, but were regarded as likely inactive due to suspected auto-fluorescence, which was observed in the initial background read. A total of 2,485 compounds were categorized as active FEN1 inhibitors and as part of the NIH Molecular Libraries Program (<https://commonfund.nih.gov/molecularlibraries>) profiled for their effect in over 150 biochemical and cell-based assays. Furthermore, cheminformatics filters were applied to the chemical library to annotate compounds for their reactivity (28). See also PubChem AID: 488816, 588795 and 720498.

### Reduced Representation Bisulfite Sequencing and analyses

The methylation landscape MCF-7 cells was determined using Reduced Representation Bisulfite Sequencing (RRBS). Bisulfite treated DNA was prepared using the Premium RRBS Kit from Diagenode (C02030032). Sequences were generated with an Illumina HiSeq 2500 (using 65 bp reads) and aligned to a bisulfite-converted Human Reference Genome Hg19 with Bismark v0.14.6 (64), using bowtie 2-2.2.5 (65) and samtools-1.3 (66). The Bismark methylation extractor was run to obtain methylation scores per cytosine. Methylation scores were processed using the bsseq package to determine differentially methylated regions between E2 and control. Regions containing <10 methylation sites or a mean difference <0.2 were omitted from further analyses. Differentially methylated regions in the near vicinity of ER $\alpha$  chromatin interactions (<20kb) were analysed as ER $\alpha$ -associated regions. The genomic distribution of RRBS regions were analysed using the cis-regulatory element annotation system (CEAS) (67). RRBS data can be found on GEO: GSE95302. Characteristics of paired RRBS samples.

| Sample                    | Total count | tag # tags after filtering | % of tags after filtering |
|---------------------------|-------------|----------------------------|---------------------------|
| Control vehicle repl1     | 22988934    | 19945060                   | 86,8                      |
| Control estradiol repl1   | 18942001    | 16422184                   | 86,7                      |
| Inhibitor vehicle repl1   | 22757385    | 19751457                   | 86,8                      |
| Inhibitor estradiol repl1 | 38067207    | 32952601                   | 86,6                      |
| Control vehicle repl2     | 30460112    | 26387978                   | 86,6                      |
| Inhibitor vehicle repl2   | 19841342    | 17211823                   | 86,7                      |
| Inhibitor estradiol repl2 | 31047474    | 26898577                   | 86,6                      |

### **Primary ex-vivo tumor cultures**

Breast tumor samples and relevant clinical data were obtained from women undergoing surgery at the Burnside Private Hospital, Adelaide, South Australia, with informed, written consent. This study was approved by the University of Adelaide Human Research Ethics Committee (approval numbers: H-065-2005; H-169-2011). Following surgery, excised tissue samples were cultured ex vivo as described previously (42, 43). Briefly, tumor pieces were cultured on gelatin sponges in full medium containing a vehicle, FEN1 inhibitor (200 nM) or, when enough material was present, tamoxifen (2 µM). After 3 to 6 days, tissue was fixed in 4% formalin in phosphate-buffered saline (PBS) at 4 °C overnight and subsequently processed into paraffin blocks. Slices (2 µm) were stained with haematoxylin and eosin or Ki67 and examined by a pathologist to confirm the presence/proportion of tumor cells. Tumor slides were scored by a pathologist for the percentage of Ki67 positive tumor cells.

### **Author contributions**

Conceptualization, K.D.F and W.Z.; Methodology, K.D.F, M.P., S.A., D.D., A.J., D.M.WIII., A.S., T.E.H., W.D.T. and W.Z.; Validation, A.J. and J.W.; Formal Analysis, K.D.F., A.J. and S.C.; Inhibitor Screening and Analysis, D.D., A.J., A.V.Z., D.M.WIII.; Investigation, K.D.F, M.P., H.P., A.J., T.E.H. and M.O.; Resources, A.S. and S.C.L.; Writing Final Draft, K.D.F. and W.Z., with help of all authors; Visualization, K.D.F. and W.Z.; Supervision, S.A., A.S., L.F.A.W., W.D.T. and W.Z.; Funding Acquisition, W.D.T. , D.M.WIII., A.S., S.A. and W.Z.

### **Acknowledgments**

The authors thank the Dutch Cancer Society KWF, Netherlands Organisation for Scientific Research (NWO), A Sister's Hope, the National Center for Advancing Translational Sciences, National Institutes of Health, National Institute on Aging and the NIH grant R03 MH092154-01 for financial support. W.D.T. and T.E.H. are supported by grants from the National Health and Medical Research Council of Australia (ID 1084416; ID 20160711) and Cancer Australia / National Breast Cancer Foundation (ID CA1043497). T.E.H. is supported by a Fellowship from the Royal Adelaide Hospital Research Foundation. The authors thank Ron Kerkhoven from the NKI Genomics Core Facility. The authors thank Sheila Stewart (Department of Cell Biology and Physiology, Washington University in St. Louis, USA) for providing pShut-

tle-FEN1hWT and pShuttle-D181A, Robert Nicholson (Cardiff School of Pharmacy and Pharmaceutical Science, Cardiff University, UK) for providing the TAM-R cells, Kenneth Nephew (Indiana University, School of Medicine, USA) for providing MCF7-T cells. The authors thank Hongmao Sun and David Maloney (National Center for Advancing Translational Sciences, National Institutes of Health, USA) for the additional design and analyses of the FEN1 HTS inhibitor screen and synthesis of required protein and reagents. The authors report no conflict of interest.

## References

1. Glass CK, Rose DW, Rosenfeld MG. Nuclear receptor coactivators. *Curr Opin Cell Biol.* 1997;9(2):222-32.
2. Jordan VC, Murphy CS. Endocrine pharmacology of antiestrogens as anti-tumor agents. *Endocrine reviews.* 1990;11(4):578-610.
3. Shou J, Massarweh S, Osborne CK, Wakeling AE, Ali S, Weiss H, et al. Mechanisms of tamoxifen resistance: increased estrogen receptor-HER2/neu cross-talk in ER/HER2-positive breast cancer. *J Natl Cancer Inst.* 2004;96(12):926-35.
4. Zwart W, Theodorou V, Kok M, Canisius S, Linn S, Carroll JS. Oestrogen receptor-co-factor-chromatin specificity in the transcriptional regulation of breast cancer. *EMBO J.* 2011;30(23):4764-76.
5. Fong YW, Cattoglio C, Tjian R. The intertwined roles of transcription and repair proteins. *Molecular cell.* 2013;52(3):291-302.
6. Periyasamy M, Patel H, Lai CF, Nguyen VT, Nevedomskaya E, Harrod A, et al. APOBEC3B-Mediated Cytidine Deamination Is Required for Estrogen Receptor Action in Breast Cancer. *Cell Rep.* 2015;13(1):108-21.
7. Krokan HE, Bjoras M. Base excision repair. *Cold Spring Harbor perspectives in biology.* 2013;5(4):a012583.
8. Zheng L, Shen B. Okazaki fragment maturation: nucleases take centre stage. *Journal of molecular cell biology.* 2011;3(1):23-30.
9. Singh P, Yang M, Dai H, Yu D, Huang Q, Tan W, et al. Overexpression and hypomethylation of flap endonuclease 1 gene in breast and other cancers. *Molecular cancer research : MCR.* 2008;6(11):1710-7.
10. Schultz-Norton JR, Walt KA, Ziegler YS, McLeod IX, Yates JR, Raetzman LT, et al. The deoxyribonucleic acid repair protein flap endonuclease-1 modulates estrogen-responsive gene expression. *Molecular endocrinology.* 2007;21(7):1569-80.
11. Abdel-Fatah TM, Russell R, Albarakati N, Maloney DJ, Dorjsuren D, Rueda OM, et al. Genomic and protein expression analysis reveals flap endonuclease 1 (FEN1) as a key biomarker in breast and ovarian cancer. *Mol Oncol.* 2014.

## Composition of ER $\alpha$ 's transcriptional complex – part 2

12. Tibshirani R, Hastie T, Narasimhan B, Chu G. Diagnosis of multiple cancer types by shrunken centroids of gene expression. *Proc Natl Acad Sci U S A*. 2002;99(10):6567-72.
13. Friedman J, Hastie T, Tibshirani R. Regularization Paths for Generalized Linear Models via Coordinate Descent. *Journal of statistical software*. 2010;33(1):1-22.
14. Loi S, Haibe-Kains B, Desmedt C, Lallemand F, Tutt AM, Gillet C, et al. Definition of clinically distinct molecular subtypes in estrogen receptor-positive breast carcinomas through genomic grade. *J Clin Oncol*. 2007;25(10):1239-46.
15. Buffa FM, Camps C, Winchester L, Snell CE, Gee HE, Sheldon H, et al. microRNA-associated progression pathways and potential therapeutic targets identified by integrated mRNA and microRNA expression profiling in breast cancer. *Cancer Res*. 2011;71(17):5635-45.
16. Curtis C, Shah SP, Chin SF, Turashvili G, Rueda OM, Dunning MJ, et al. The genomic and transcriptomic architecture of 2,000 breast tumours reveals novel subgroups. *Nature*. 2012;486(7403):346-52.
17. Kok M, Koornstra RH, Margarido TC, Fles R, Armstrong NJ, Linn SC, et al. Mammosphere-derived gene set predicts outcome in patients with ER-positive breast cancer. *J Pathol*. 2009;218(3):316-26.
18. Michalides R, van Tinteren H, Balkenende A, Vermorken JB, Benraadt J, Huldij J, et al. Cyclin A is a prognostic indicator in early stage breast cancer with and without tamoxifen treatment. *Br J Cancer*. 2002;86(3):402-8.
19. Beelen K, Zwart W, Linn SC. Can predictive biomarkers in breast cancer guide adjuvant endocrine therapy? *Nat Rev Clin Oncol*. 2012;9(9):529-41.
20. Zheng L, Jia J, Finger LD, Guo Z, Zer C, Shen B. Functional regulation of FEN1 nuclease and its link to cancer. *Nucleic acids research*. 2011;39(3):781-94.
21. Saharia A, Teasley DC, Duxin JP, Dao B, Chiappinelli KB, Stewart SA. FEN1 ensures telomere stability by facilitating replication fork re-initiation. *The Journal of biological chemistry*. 2010;285(35):27057-66.
22. van Pel DM, Barrett IJ, Shimizu Y, Sajesh BV, Guppy BJ, Pfeifer T, et al. An evolutionarily conserved synthetic lethal interaction network identifies FEN1 as a broad-spectrum target for anticancer therapeutic development. *PLoS genetics*. 2013;9(1):e1003254.
23. Tumey LN, Bom D, Huck B, Gleason E, Wang J, Silver D, et al. The identification and optimization of a N-hydroxy urea series of flap endonuclease 1 inhibitors. *Bioorg Med Chem Lett*. 2005;15(2):277-81.
24. Exell JC, Thompson MJ, Finger LD, Shaw SJ, Debreczeni J, Ward TA, et al. Cellularly active N-hydroxyurea FEN1 inhibitors block substrate entry to the active

site. *Nature chemical biology*. 2016;12(10):815-21.

25. Dorjsuren D, Kim D, Maloney DJ, Wilson DM, 3rd, Simeonov A. Complementary non-radioactive assays for investigation of human flap endonuclease 1 activity. *Nucleic acids research*. 2011;39(2):e11.

26. Inglese J, Auld DS, Jadhav A, Johnson RL, Simeonov A, Yasgar A, et al. Quantitative high-throughput screening: a titration-based approach that efficiently identifies biological activities in large chemical libraries. *Proc Natl Acad Sci U S A*. 2006;103(31):11473-8.

27. Yasgar A, Shinn P, Jadhav A, Auld D, Michael S, Zheng W, et al. Compound Management for Quantitative High-Throughput Screening. *Jala*. 2008;13(2):79-89.

28. Jadhav A, Ferreira RS, Klumpp C, Mott BT, Austin CP, Inglese J, et al. Quantitative analyses of aggregation, autofluorescence, and reactivity artifacts in a screen for inhibitors of a thiol protease. *Journal of medicinal chemistry*. 2010;53(1):37-51.

29. Zhang F, Wang Y, Wang L, Luo X, Huang K, Wang C, et al. Poly(ADP-ribose) polymerase 1 is a key regulator of estrogen receptor alpha-dependent gene transcription. *The Journal of biological chemistry*. 2013;288(16):11348-57.

30. Ju BG, Lunyak VV, Perissi V, Garcia-Bassets I, Rose DW, Glass CK, et al. A topoisomerase IIbeta-mediated dsDNA break required for regulated transcription. *Science*. 2006;312(5781):1798-802.

31. Lee HS, Park JH, Kim SJ, Kwon SJ, Kwon J. A cooperative activation loop among SWI/SNF, gamma-H2AX and H3 acetylation for DNA double-strand break repair. *EMBO J*. 2010;29(8):1434-45.

32. Nawaz Z, Lonard DM, Dennis AP, Smith CL, O'Malley BW. Proteasome-dependent degradation of the human estrogen receptor. *Proc Natl Acad Sci U S A*. 1999;96(5):1858-62.

33. Ung M, Ma X, Johnson KC, Christensen BC, Cheng C. Effect of estrogen receptor alpha binding on functional DNA methylation in breast cancer. *Epigenetics*. 2014;9(4):523-32.

34. Kangaspeska S, Stride B, Metivier R, Polycarpou-Schwarz M, Ibberson D, Carmouche RP, et al. Transient cyclical methylation of promoter DNA. *Nature*. 2008;452(7183):112-5.

35. Bhutani N, Burns DM, Blau HM. DNA demethylation dynamics. *Cell*. 2011;146(6):866-72.

36. Meissner A, Gnirke A, Bell GW, Ramsahoye B, Lander ES, Jaenisch R. Reduced representation bisulfite sequencing for comparative high-resolution DNA methylation analysis. *Nucleic acids research*. 2005;33(18):5868-77.

37. Hurtado A, Holmes KA, Ross-Innes CS, Schmidt D, Carroll JS. FOXA1 is a key determinant of estrogen receptor function and endocrine response. *Nature genet-*

## Composition of ER $\alpha$ 's transcriptional complex – part 2

*ics*. 2011;43(1):27-33.

38. Robinson DR, Wu YM, Vats P, Su F, Lonigro RJ, Cao X, et al. Activating ESR1 mutations in hormone-resistant metastatic breast cancer. *Nature genetics*. 2013;45(12):1446-51.

39. Jeong KW, Kim K, Situ AJ, Ulmer TS, An W, Stallcup MR. Recognition of enhancer element-specific histone methylation by TIP60 in transcriptional activation. *Nature structural & molecular biology*. 2011;18(12):1358-65.

40. Fan M, Yan PS, Hartman-Frey C, Chen L, Paik H, Oyer SL, et al. Diverse gene expression and DNA methylation profiles correlate with differential adaptation of breast cancer cells to the antiestrogens tamoxifen and fulvestrant. *Cancer Res*. 2006;66(24):11954-66.

41. Knowlden JM, Hutcheson IR, Jones HE, Madden T, Gee JM, Harper ME, et al. Elevated levels of epidermal growth factor receptor/c-erbB2 heterodimers mediate an autocrine growth regulatory pathway in tamoxifen-resistant MCF-7 cells. *Endocrinology*. 2003;144(3):1032-44.

42. Dean JL, McClendon AK, Hickey TE, Butler LM, Tilley WD, Witkiewicz AK, et al. Therapeutic response to CDK4/6 inhibition in breast cancer defined by ex vivo analyses of human tumors. *Cell cycle*. 2012;11(14):2756-61.

43. Mohammed H, Russell IA, Stark R, Rueda OM, Hickey TE, Tarulli GA, et al. Progesterone receptor modulates ER $\alpha$  action in breast cancer. *Nature*. 2015;523(7560):313-7.

44. Dai X, Li T, Bai Z, Yang Y, Liu X, Zhan J, et al. Breast cancer intrinsic subtype classification, clinical use and future trends. *Am J Cancer Res*. 2015;5(10):2929-43.

45. DiRenzo J, Shang Y, Phelan M, Sif S, Myers M, Kingston R, et al. BRG-1 is recruited to estrogen-responsive promoters and cooperates with factors involved in histone acetylation. *Molecular and cellular biology*. 2000;20(20):7541-9.

46. Perillo B, Ombra MN, Bertoni A, Cuzzo C, Sacchetti S, Sasso A, et al. DNA oxidation as triggered by H3K9me2 demethylation drives estrogen-induced gene expression. *Science*. 2008;319(5860):202-6.

47. Gong C, Fujino K, Monteiro LJ, Gomes AR, Drost R, Davidson-Smith H, et al. FOXA1 repression is associated with loss of BRCA1 and increased promoter methylation and chromatin silencing in breast cancer. *Oncogene*. 2015;34(39):5012-24.

48. Stone A, Zotenko E, Locke WJ, Korbie D, Millar EK, Pidsley R, et al. DNA methylation of oestrogen-regulated enhancers defines endocrine sensitivity in breast cancer. *Nature communications*. 2015;6:7758.

49. Ma J, Wang M. Interplay between DNA supercoiling and transcription elongation. *Transcription*. 2014;5(3):e28636.

50. Santos-Pereira JM, Aguilera A. R loops: new modulators of genome dynamics and function. *Nature reviews Genetics*. 2015;16(10):583-97.
51. Stork CT, Bocek M, Crossley MP, Sollier J, Sanz LA, Chedin F, et al. Co-transcriptional R-loops are the main cause of estrogen-induced DNA damage. *eLife*. 2016;5.
52. He L, Zhang Y, Sun H, Jiang F, Yang H, Wu H, et al. Targeting DNA Flap Endonuclease 1 to Impede Breast Cancer Progression. *EBioMedicine*. 2016.
53. Panda H, Jaiswal AS, Corsino PE, Armas ML, Law BK, Narayan S. Amino acid Asp181 of 5'-flap endonuclease 1 is a useful target for chemotherapeutic development. *Biochemistry*. 2009;48(42):9952-8.
54. McManus KJ, Barrett IJ, Nouhi Y, Hieter P. Specific synthetic lethal killing of RAD54B-deficient human colorectal cancer cells by FEN1 silencing. *Proc Natl Acad Sci U S A*. 2009;106(9):3276-81.
55. Giresi PG, Lieb JD. Isolation of active regulatory elements from eukaryotic chromatin using FAIRE (Formaldehyde Assisted Isolation of Regulatory Elements). *Methods*. 2009;48(3):233-9.
56. Jansen MP, Knijnenburg T, Reijm EA, Simon I, Kerkhoven R, Droog M, et al. Hallmarks of aromatase inhibitor drug resistance revealed by epigenetic profiling in breast cancer. *Cancer Res*. 2013;73(22):6632-41.
57. Zhang Y, Liu T, Meyer CA, Eeckhoute J, Johnson DS, Bernstein BE, et al. Model-based analysis of ChIP-Seq (MACS). *Genome biology*. 2008;9(9):R137.
58. Kumar V, Muratani M, Rayan NA, Kraus P, Lufkin T, Ng HH, et al. Uniform, optimal signal processing of mapped deep-sequencing data. *Nature biotechnology*. 2013;31(7):615-22.
59. Ye T, Krebs AR, Choukrallah MA, Keime C, Plewniak F, Davidson I, et al. seqMINER: an integrated ChIP-seq data interpretation platform. *Nucleic acids research*. 2011;39(6):e35.
60. Lopez-Garcia J, Periyasamy M, Thomas RS, Christian M, Leao M, Jat P, et al. ZNF366 is an estrogen receptor corepressor that acts through CtBP and histone deacetylases. *Nucleic acids research*. 2006;34(21):6126-36.
61. Kok M, Linn SC, Van Laar RK, Jansen MP, van den Berg TM, Delahaye LJ, et al. Comparison of gene expression profiles predicting progression in breast cancer patients treated with tamoxifen. *Breast cancer research and treatment*. 2009;113(2):275-83.
62. Beelen K, Opdam M, Severson TM, Koornstra RH, Vincent AD, Wesseling J, et al. Phosphorylated p-70S6K predicts tamoxifen resistance in postmenopausal breast cancer patients randomized between adjuvant tamoxifen versus no systemic treatment. *Breast cancer research : BCR*. 2014;16(1):R6.

## Composition of ER $\alpha$ 's transcriptional complex – part 2

63. Michael S, Auld D, Klumpp C, Jadhav A, Zheng W, Thorne N, et al. A robotic platform for quantitative high-throughput screening. *Assay and drug development technologies*. 2008;6(5):637-57.
64. Krueger F, Andrews SR. Bismark: a flexible aligner and methylation caller for Bisulfite-Seq applications. *Bioinformatics*. 2011;27(11):1571-2.
65. Langmead B, Salzberg SL. Fast gapped-read alignment with Bowtie 2. *Nature methods*. 2012;9(4):357-9.
66. Li H, Handsaker B, Wysoker A, Fennell T, Ruan J, Homer N, et al. The Sequence Alignment/Map format and SAMtools. *Bioinformatics*. 2009;25(16):2078-9.
67. Ji X, Li W, Song J, Wei L, Liu XS. CEAS: cis-regulatory element annotation system. *Nucleic acids research*. 2006;34(Web Server issue):W551-4.

## Supplementary information

### Figure S1.

(A) Heatmap showing the correlation of the four individual genes with the disease specific survival of breast cancer patients from METABRIC stratified by ER $\alpha$  status. Discovery (n=827) and validation (n=822) cohorts were analyzed separately. Heatmap values are from an adjusted cox-regression where a color gradient (upper limit log (HR>2), middle limit log (HR=1) and lower limit log (HR=0.4)) was used. Multivariate significant results are in bold with a green border, whereas non-significant results are transparent. (B) Disease specific survival of breast cancer patients over time (days) categorized according to FEN1 expression levels in the METABRIC discovery and validation set. Additionally patients were stratified according to ER $\alpha$  status. The median of FEN1 expression was used as a cut-off to divide patients in a Low expression group (blue) and a High expression group (green). Adjusted cox-regression is shown. (C) As in B, but now ER $\alpha$ -positive patients which received hormonal therapy were included and the validation and discovery cohorts were merged. Log-rank, cox-regression and interaction test between FEN1 levels and hormonal therapy are shown. (D) As in B, but now patients were stratified according to menopausal status and the validation and discovery cohorts were merged. Log-rank and cox-regression are shown.

### Figure S2.

(A) Western blot analyses after siRNA targeting or overexpression of FEN1. Protein levels were determined for ER $\alpha$ , endogenous FEN1 and exogenous FLAG-tagged FEN1. Actin was used as loading control. Cells were treated with (+) or without (-) estradiol overnight before lysis. (B) Western blot analyses of cells used for ER $\alpha$ ,

p300 and FOXA1 ChIP-seq and ER $\alpha$  ChIP-qPCR after siRNA targeting or overexpression of FEN1. Protein levels were determined for ER $\alpha$ , p300, FOXA1, endogenous FEN1 and exogenous FLAG-tagged FEN1. Actin and RNA Pol II were used as loading control. Blots depicting samples used for Figure 2C,D,E are labelled ER $\alpha$ /p300 and FOXA1 ChIP-seq, whereas samples used for Figure 2G are labelled ER $\alpha$ -ChIP. (C) ChIP-qPCR validation of FOXA1, ER $\alpha$  and p300 ChIP-seq at enhancer regions proximal to GREB1, XBP1 and RARA. Additionally a RNA Pol II ChIP-qPCR was performed. Signals for each primer set are normalized over control regions and siControl (blue), which is set as 1. Shown is an example of two biological replicates.  $N=4$  with mean  $\pm$  SD.  $*=p\text{-value}<0.01$  Students T-test.

### Figure S3.

(A) Deconvolution of pool of siRNA targeting FEN1. (Left) Western blot analyses after siRNA targeting by individual siRNA's or by a pool of 4 (siFEN1 pool). Protein levels were determined for FEN1 and actin, which was used as loading control. Quantified FEN1-protein levels as normalized over loading control actin are shown. (Right) Relative cell growth (Y-axis) of MCF-7 cells treated with estradiol. Cells were transfected with siControl or the individual FEN1 siRNA's. Relative growth was normalized over the plate confluency at timepoint 0. Shown is a representative experiment of two biological replicates.  $N=6$  with mean  $\pm$  SD.  $*=p\text{-value}<0.05$  (B) Relative cell growth (Y-axis) of T47D cells treated with vehicle control, E2, tamoxifen or fulvestrant. Cells were transfected with control siControl (blue) or siFEN1 (red). Relative growth was normalized over the plate confluency at timepoint 0. Shown is a representative experiment of three biological replicates.  $N=6$  with mean  $\pm$  SD.  $*=p\text{-value}<0.05$  and  $***=p\text{-value}<0.001$  Students T-test.

### Figure S4.

(A) Altered FEN1 enzyme activity at the maximum tested concentration of 465,195 screened compounds. The percentage of altered FEN1 enzyme activity (Y-axis) at the maximum tested concentration of all screened compounds (X-axis). Compounds are divided into active inhibitors (green), inconclusive compounds (yellow) and inactive compounds (blue). The top hit from our biological validations, MLS002701801 (red), has been highlighted. (B) Relative cell proliferation (Y-axis) over time (X-axis) of MCF-7 cells treated with a vehicle or 10  $\mu$ M of each of the three inhibitors. Shown is an example of two biological replicates.  $N=6$  with mean  $\pm$  SD. (C) Colony formation assay of ER $\alpha$ -negative cell lines MDA-MB-231 and CAL-120. Cells were treated with the minimum compound concentrations still capable of proficient MCF-7 growth inhibition. Representative experiment is shown of two biological experi-

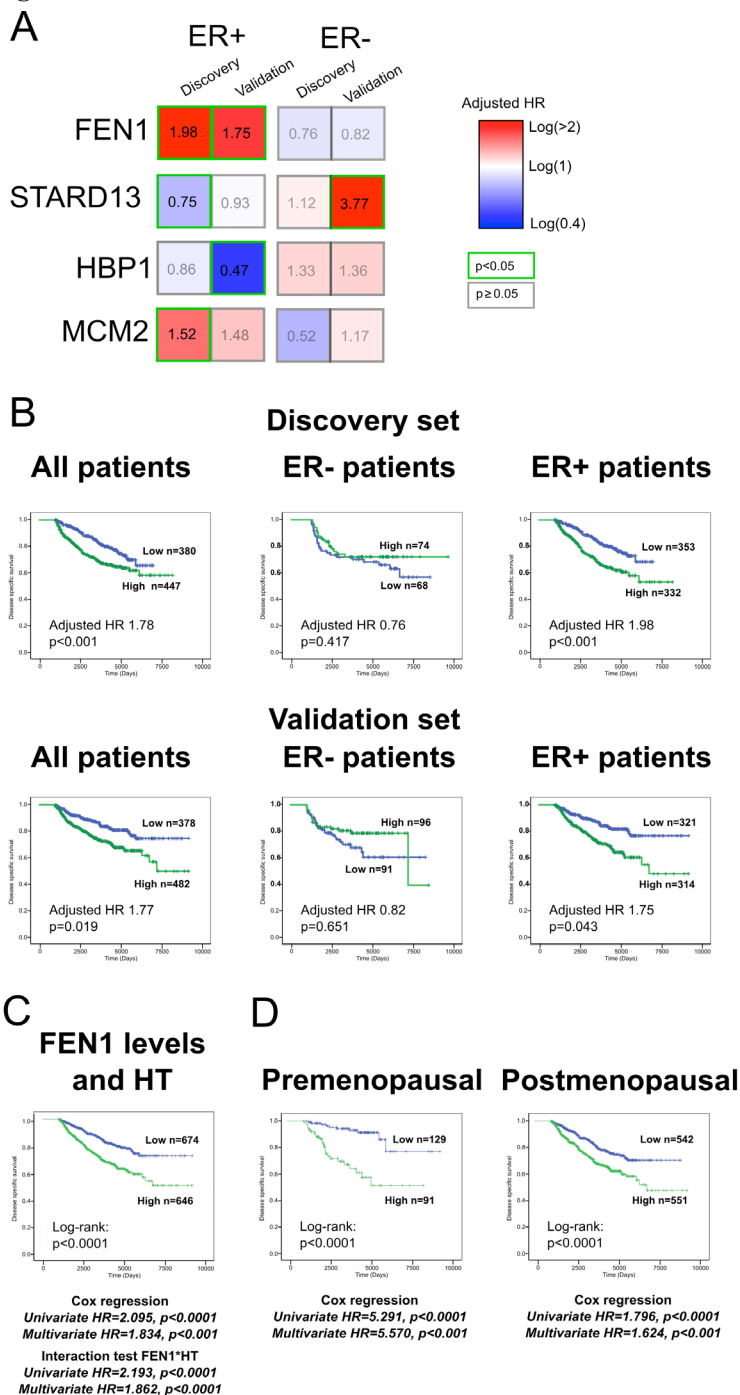
## Composition of ER $\alpha$ 's transcriptional complex – part 2

ments. (D) ChIP-qPCR validation of PARP1 and XRCC1 ChIP-seq at ER $\alpha$ -bound enhancer regions proximal to TFF1, GREB1, XBP1 and RARA. Two regions negative for ER $\alpha$  binding were used as negative controls (blue). Shown is an example of two biological replicates. Depicted is the percentage of input with N=4 with mean  $\pm$  SD. \*\*\*=p-value<0.001 Students T-test. (E) Bar graph depicting the percentage of  $\gamma$ H2AX-foci positive cells (n=500) on immunofluorescence. Hormone-deprived cells were treated with ethanol control or estradiol for 15 minutes, with or without FEN1 inhibitor. Shown is a representative experiment of two biological replicates. (F) ChIP-qPCR validation of ER $\alpha$ , PARP1 and BRG1 ChIP-seq at ER $\alpha$ -bound enhancer regions proximal to TFF1, GREB1 and XBP1. Signals for each primer set are normalized over control regions. Shown is an example of two biological replicates. N=4 (ER $\alpha$  and PARP1) or N=5 (BRG1) with mean  $\pm$  SD. \*=p-value<0.05, \*\*=p-value<0.01 and \*\*\*=p-value<0.001 Students T-test. (G) (Left) Western blot depicting ER $\alpha$ , FEN1 and actin protein levels. Hormone-deprived cells were pretreated overnight with or without FEN1 inhibitor and treated three hours with 10 $\mu$ M of MG132 when appropriate before stimulation with estradiol. Shown is an example experiment of two biological replicates with quantified ER $\alpha$ -protein levels as normalized over loading control actin. (Right) ChIP-qPCR of ER $\alpha$  at enhancer regions proximal to TFF1, GREB1 and XBP1. Cells were pretreated overnight with or without FEN1 inhibitor and treated three hours with 10 $\mu$ M of MG132 before 30 minutes of estradiol stimulation. Signals for each primer set are normalized over negative control region. Shown is an example of two biological replicates. N=4 with mean  $\pm$  SD. \*=p-value<0.05 Students T-test.

### Figure S5.

(A) ChIP-qPCR ER $\alpha$  at enhancer regions proximal to TFF1, GREB1 and XBP1. Hormone deprived cells were treated with 0, 15, 30 or 45 minutes of estradiol prior to fixation. Signals for each primer set are normalized over negative control region. Shown is an example of two biological replicates. N=4 with mean  $\pm$  SD. (B) Left: Western Blot depicting ER $\alpha$  and FEN1 protein levels with actin as a control after pretreatment with the FEN1 inhibitor. In the absence of estradiol stimulation ER $\alpha$  protein levels are unaffected by the FEN1 inhibitor, indicating that the subsequent decrease in ER $\alpha$ -chromatin interactions or ER $\alpha$ -activity are not due to decreased starting amounts of the ER $\alpha$  protein. Representative blot of three biological experiments is shown. Right: Normalized quantification of ER $\alpha$  protein levels of the three biological replicates. N=3 with mean  $\pm$  SEM. (C) Indication of the percentage of Ki67 positive tumor cells in tumor explants cultured in the presence or absence of FEN1 inhibitor or tamoxifen.

Figure S1.



Composition of ER $\alpha$ 's transcriptional complex – part 2

Figure S2.

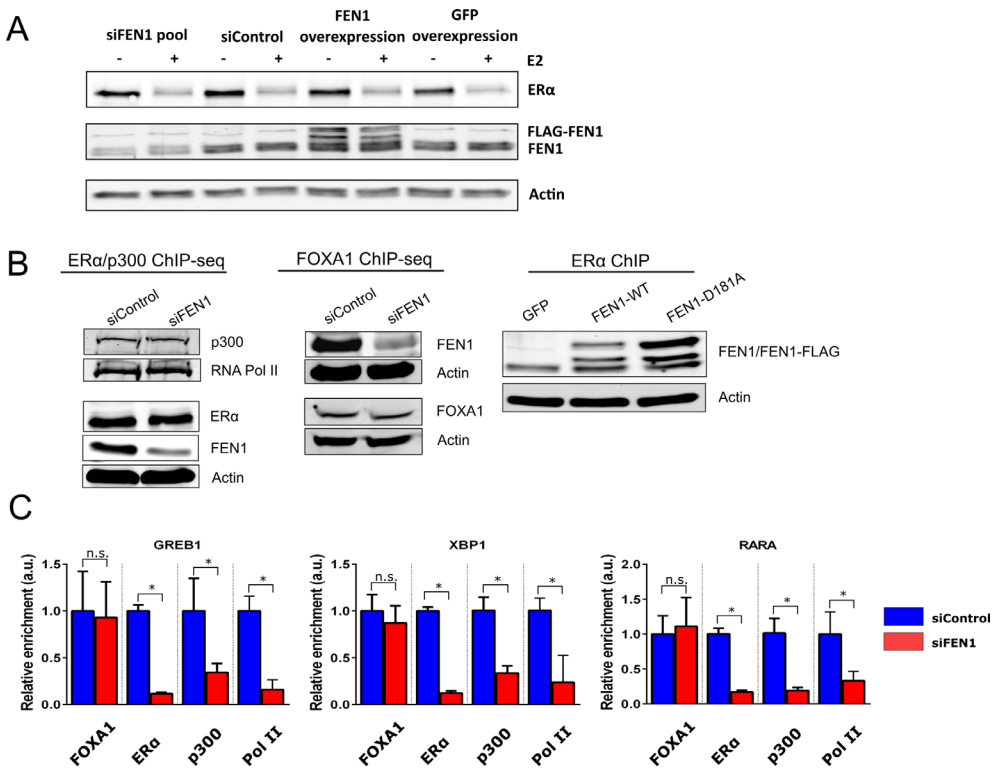


Figure S3.

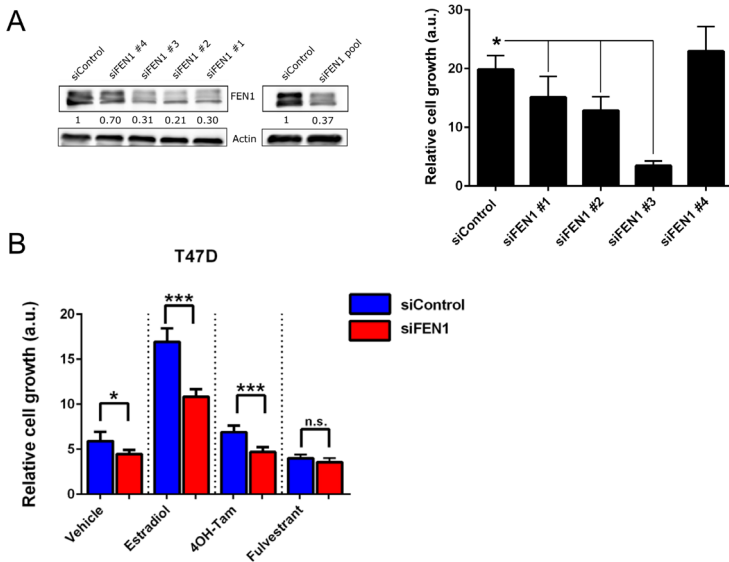
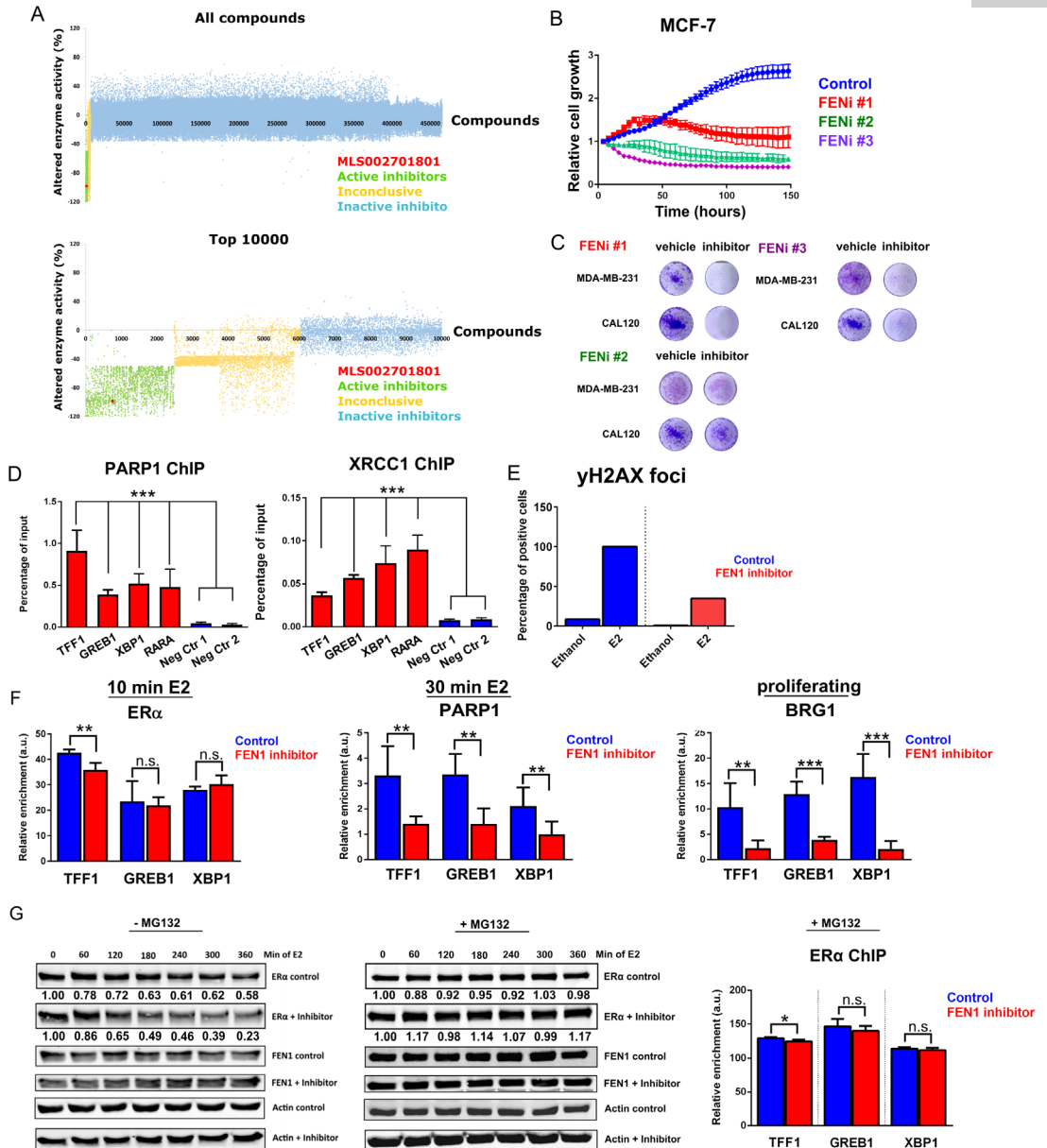


Figure S4.



Composition of ER $\alpha$ 's transcriptional complex – part 2

Figure S5.

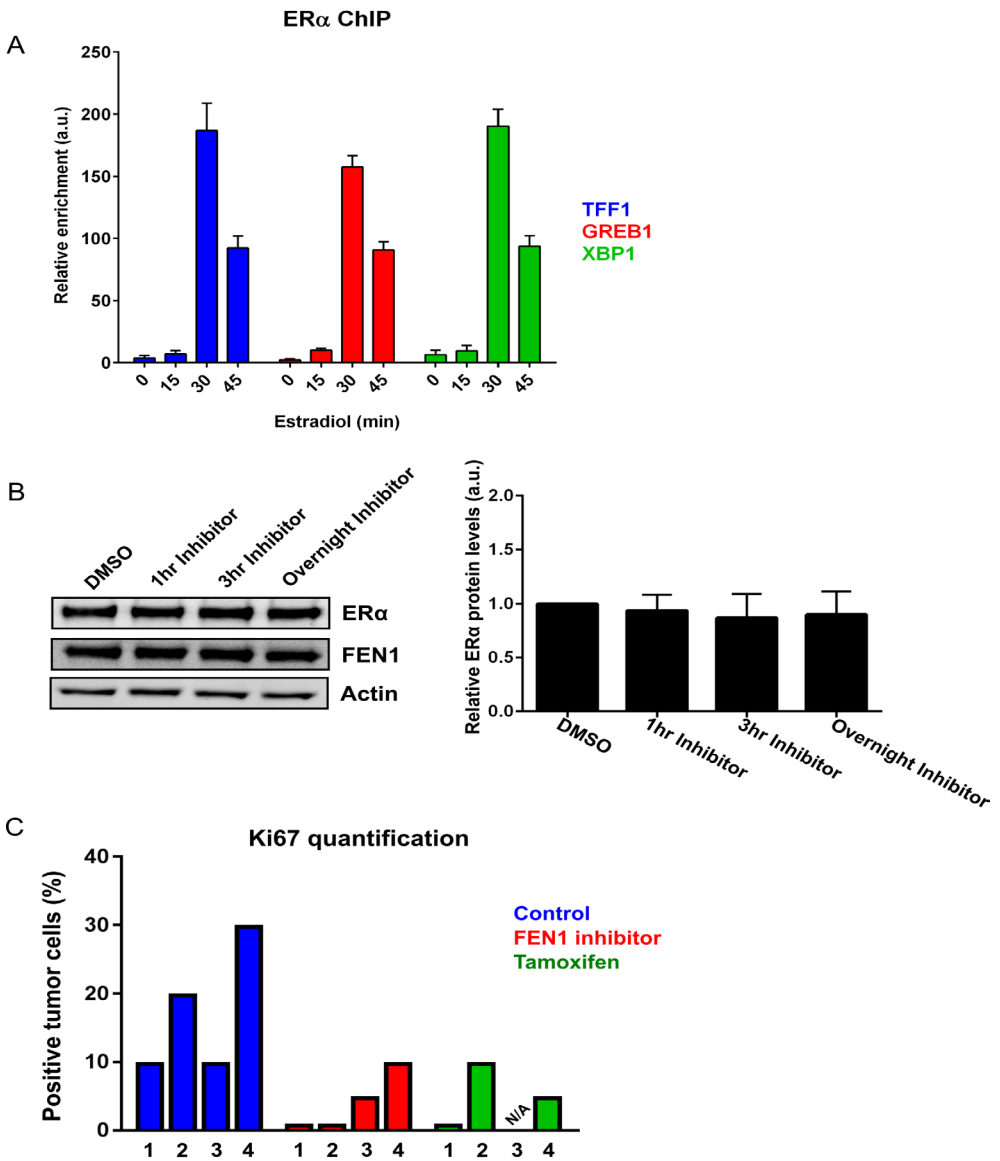


Table S1.

**Discovery cohort***Multivariate analyses FEN1 mRNA*

| Variable                                       | Hazard ratio (95% CI) | p-value |
|--|-----------------------|---------|
| <b>FEN1 mRNA levels</b>                        | 2.02 (0.91-4.49)      | 0.084   |
| <b>Age (&lt;60 versus <math>\geq</math>60)</b> | 0.71 (0.35-1.43)      | 0.333   |
| <b>Affected Lymph nodes none</b>               |                       | 0.015   |
| 1-3  | 1.58 (0.54-4.64)      | 0.408   |
| $\geq$ 4                                       | 3.94 (1.24-12.50)     | 0.020   |
| <b>Tumor diameter <math>\leq</math>20 mm</b>   |                       | 0.297   |
| 20-50 mm                                       | 1.71 (0.80-3.68)      | 0.169   |
| >50 mm   | 2.59 (0.52-12.83)     | 0.244   |
| <b>Tumor Grade Grade 1</b>                     |                       | 0.827   |
| Grade 2  | 1.29 (0.57-2.94)      | 0.539   |
| Grade 3  | 1.19 (0.40-3.53)      | 0.749   |

*Multivariate analyses FEN1 IHC*

| Variable                                       | Hazard ratio (95% CI) | p-value |
|--|-----------------------|---------|
| <b>FEN1 IHC score</b>                          | 1.61 (0.77-3.35)      | 0.205   |
| <b>Age (&lt;60 versus <math>\geq</math>60)</b> | 0.69 (0.33-1.45)      | 0.325   |
| <b>Affected Lymph nodes none</b>               |                       | 0.030   |
| 1-3  | 1.38 (0.46-4.13)      | 0.565   |
| $\geq$ 4                                       | 3.30 (1.05-10.36)     | 0.041   |
| <b>Tumor diameter <math>\leq</math>20 mm</b>   |                       | 0.057   |
| 20-50 mm                                       | 2.83 (1.21-6.62)      | 0.017   |
| >50 mm   | 2.16 (0.41-11.32)     | 0.361   |
| <b>Tumor Grade Grade 1</b>                     |                       | 0.962   |
| Grade 2  | 1.12 (0.50-2.51)      | 0.786   |
| Grade 3  | 1.05 (0.38-2.94)      | 0.921   |

**Validation cohort***Multivariate analyses FEN1 in ER $\alpha$  negative patients*

| Variable                                       | Hazard ratio (95% CI) | p-value |
|--|-----------------------|---------|
| <b>FEN1 IHC score</b>                          | 1.20 (0.69-2.09)      | 0.514   |
| <b>Age (&lt;65 versus <math>\geq</math>65)</b> | 0.45 (0.24-0.82)      | 0.009   |
| <b>Tumor Grade (grade 1-2 versus grade 3)</b>  | 1.12 (0.61-2.04)      | 0.718   |
| <b>Tumor Stage (T1-T2 versus T3-T4)</b>        | 2.83 (1.41-5.71)      | 0.004   |
| <b>HER2 status (Negative versus positive)</b>  | 1.54 (0.86-2.77)      | 0.145   |
| <b>PgR status (Negative versus positive)</b>   | 1.21 (0.36-4.07)      | 0.761   |

*Multivariate analyses FEN1 in ER $\alpha$  positive patients*

| Variable                                       | Hazard ratio (95% CI) | p-value |
|--|-----------------------|---------|
| <b>FEN1 IHC score</b>                          | 1.58 (1.01-2.47)      | 0.047   |
| <b>Age (&lt;65 versus <math>\geq</math>65)</b> | 1.03 (0.68-1.57)      | 0.874   |
| <b>Tumor Grade (grade 1-2 versus grade 3)</b>  | 1.87 (1.19-2.94)      | 0.006   |
| <b>Tumor Stage (T1-T2 versus T3-T4)</b>        | 1.74 (1.04-2.92)      | 0.035   |
| <b>HER2 status (Negative versus positive)</b>  | 1.12 (0.60-2.08)      | 0.722   |
| <b>PgR status (Negative versus positive)</b>   | 1.13 (0.74-1.71)      | 0.579   |

*Multivariate analyses FEN1 in no adjuvant treatment patients*

| Variable                                       | Hazard ratio (95% CI) | p-value |
|--|-----------------------|---------|
| <b>FEN1 IHC score</b>                          | 1.59 (0.62-4.06)      | 0.336   |
| <b>Age (&lt;65 versus <math>\geq</math>65)</b> | 0.87 (0.38-2.00)      | 0.740   |

## Composition of ER $\alpha$ 's transcriptional complex – part 2

|   |                   |       |
|---|-------------------|-------|
| <b>Tumor Grade</b> (grade 1-2 versus grade 3) | 1.29 (0.47-3.56)  | 0.623 |
| <b>Tumor Stage</b> (T1-T2 versus T3-T4)       | 3.70 (1.16-11.86) | 0.028 |
| <b>HER2 status</b> (Negative versus positive) | 1.48 (0.26-8.43)  | 0.656 |
| <b>PgR status</b> (Negative versus positive)  | 0.94 (0.37-2.35)  | 0.887 |

### Multivariate analyses FEN1 in adjuvant tamoxifen patients

| Variable                                      | Hazard ratio (95% CI) | p-value |
|---|-----------------------|---------|
| <b>FEN1 IHC score</b>                         | 1.66 (0.97-2.82)      | 0.063   |
| <b>Age</b> (<65 versus $\geq$ 65)             | 1.13 (0.69-1.84)      | 0.626   |
| <b>Tumor Grade</b> (grade 1-2 versus grade 3) | 2.06 (1.22-3.48)      | 0.007   |
| <b>Tumor Stage</b> (T1-T2 versus T3-T4)       | 1.53 (0.85-2.78)      | 0.160   |
| <b>HER2 status</b> (Negative versus positive) | 1.11 (0.56-2.19)      | 0.764   |
| <b>PgR status</b> (Negative versus positive)  | 1.16 (0.71-1.88)      | 0.555   |

### Multivariate analyses in FEN1 low patients

| Variable   | Hazard ratio (95% CI) | p-value |
|--|-----------------------|---------|
| <b>Treatment</b> (tamoxifen versus no tamoxifen) | 0.39 (0.18-0.83)      | 0.015   |
| <b>Age</b> (<65 versus $\geq$ 65)                | 0.44 (0.23-0.87)      | 0.017   |
| <b>Tumor Grade</b> (grade 1-2 versus grade 3)    | 1.92 (0.94-3.94)      | 0.075   |
| <b>Tumor Stage</b> (T1-T2 versus T3-T4)          | 1.41 (0.64-3.15)      | 0.396   |
| <b>HER2 status</b> (Negative versus positive)    | 3.58 (0.94-13.60)     | 0.061   |
| <b>PgR status</b> (Negative versus positive)     | 1.13 (0.56-2.30)      | 0.735   |

### Multivariate analyses in FEN1 High patients

| Variable   | Hazard ratio (95% CI) | p-value |
|--|-----------------------|---------|
| <b>Treatment</b> (tamoxifen versus no tamoxifen) | 0.67 (0.35-1.26)      | 0.213   |
| <b>Age</b> (<65 versus $\geq$ 65)                | 1.91 (1.10-3.29)      | 0.021   |
| <b>Tumor Grade</b> (grade 1-2 versus grade 3)    | 1.85 (1.02-3.38)      | 0.045   |
| <b>Tumor Stage</b> (T1-T2 versus T3-T4)          | 1.59 (0.79-3.22)      | 0.197   |
| <b>HER2 status</b> (Negative versus positive)    | 0.95 (0.47-1.93)      | 0.884   |
| <b>PgR status</b> (Negative versus positive)     | 1.05 (0.60-1.81)      | 0.872   |

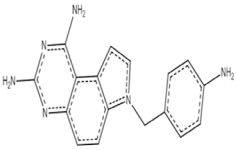
### FEN1 levels and tamoxifen interaction test

| Variable                                 | Hazard ratio (95% CI) | p-value |
|--|-----------------------|---------|
| <b>Tamoxifen treatment x FEN1 levels</b> | 1.48 (0.99-2.21)      | 0.053   |

**Table S1.** Multivariate cox-regression of FEN1 in the Discovery and Validation cohort.

Adjusted Cox proportional hazard regression analyses were performed with the following covariates; for the discovery-cohort the covariates age (<60 versus  $\geq$ 60), diameter of the tumor ( $\leq$ 20 mm versus 20-50 mm versus >50 mm), tumor grade (grade 1 versus grade 2 versus grade 3) and the number of affected lymph nodes (Negative versus 1-3 versus  $\geq$ 4), and for the validation-cohort the covariates age (< 65 versus  $\geq$  65), grade (grade 1-2 versus grade 3), tumor stage (T1-T2 versus T3-4), HER2 status (negative versus positive), PgR status (negative versus positive). Adjusted hazard ratio with 95% CI and p-value are shown. Additionally interaction test between the variable tamoxifen treatment and FEN1 levels is shown.

Table S2

| Chemical structure  | Molecular formula                              | PubChem CID                            |
|---|--|--|
|  | C <sub>17</sub> H <sub>16</sub> N <sub>6</sub> | 432465                                 |
|   | <b>Molecular Weight</b><br>304.35              | <b>registration ID</b><br>MLS002701801 |
| Assay Protocol  | IC <sub>50</sub> (μM)                          | Inhibition at 57 μM                    |
| Thiazole orange DNA binding assay   | <i>inactive</i>                                | 15.44 %                                |
| DNA Polymerase Beta activity assay  | <i>inactive</i>                                | 20.3 %                                 |
| DNA Polymerase Iota activity assay  | <i>inactive</i>                                | -15.47 %                               |
| DNA Polymerase Kappa activity assay   | <i>inactive</i>                                | -36.2 %                                |
| BRCA1 activity assay  | <i>inactive</i>                                | -1.7 %                                 |
| PCNA activity assay   | <i>inactive</i>                                | 23.14 %                                |
| WRN helicase activity assay   | <i>inactive</i>                                | 13.09 %                                |
| FEN1 activity assay - initial screen compound source 1                            | <b>1,37</b>                                    | 83.68 %                                |
| FEN1 activity assay - initial screen compound source 2                            | <b>1,22</b>                                    | 79.08 %                                |
| FEN1 activity assay - validation screen   | <b>6,75</b>                                    | 74.39 %                                |
| FEN1 activity assay - validation screen with purified sample                      | <b>1,22</b>                                    | 80.72 %                                |
| APE1 activity assay - compound source 1   | <b>25,12</b>                                   | 48.72 %                                |
| APE1 activity assay - compound source 2   | <b>28,18</b>                                   | 42.07 %                                |

**Table S2.** Characteristics of the small molecule inhibitor of FEN1.

Chemical structure and characteristics of the FEN1 inhibitor. Additionally the IC<sub>50</sub> (μM) and inhibition at the maximum tested concentration (57 μM) in multiple activity assays (NIH Molecular Libraries Program (<https://commonfund.nih.gov/molecularlibraries>)) is shown.

*Composition of ER $\alpha$ 's transcriptional complex – part 2*

**Table S3**

**FBS**

| <b>Cells</b> | <b>IC<sub>50</sub></b> | <b>Std.Error</b> | <b>CI.Lower</b> | <b>CI.Upper</b> |
|--------------|------------------------|------------------|-----------------|-----------------|
| MCF-7        | 69                     | 14               | 39              | 99              |
| T47D         | 78                     | 24               | 28              | 128             |
| MCF7-T       | 29                     | 4                | 21              | 37              |
| TAMR         | 29                     | 4                | 21              | 38              |
| CAL120       | <i>NA</i>              | <i>NA</i>        | <i>NA</i>       | <i>NA</i>       |
| BT20         | 314                    | 298              | -286            | 914             |

**Tamoxifen**

| <b>Cells</b> | <b>IC<sub>50</sub></b> | <b>Std.Error</b> | <b>CI.Lower</b> | <b>CI.Upper</b> |
|--------------|------------------------|------------------|-----------------|-----------------|
| MCF-7        | <i>NA</i>              | <i>NA</i>        | <i>NA</i>       | <i>NA</i>       |
| T47D         | <i>NA</i>              | <i>NA</i>        | <i>NA</i>       | <i>NA</i>       |
| MCF7-T       | 22                     | 4                | 13              | 31              |
| TAMR         | 23                     | 5                | 13              | 33              |
| CAL120       | <i>NA</i>              | <i>NA</i>        | <i>NA</i>       | <i>NA</i>       |
| BT20         | 895                    | 1390             | -1904           | 3694            |

**Table S3.** *IC<sub>50</sub> of FENI inhibitor for individual cell lines under full medium (FBS) or tamoxifen conditions. For cell lines reaching 50% growth inhibition, IC<sub>50</sub> was determined and depicted with 95% CI.*



